N O T I C E

THIS DOCUMENT HAS BEEN REPRODUCED FROM
MICROFICHE. ALTHOUGH IT IS RECOGNIZED THAT
CERTAIN PORTIONS ARE ILLEGIBLE, IT IS BEING RELEASED
IN THE INTEREST OF MAKING AVAILABLE AS MUCH
INFORMATION AS POSSIBLE

COMETARY PARTICULATE ANALYZER

DESIGN DEFINITION STUDY

FINAL REPORT

PREPARED FOR

NASA HEADQUARTERS
WASHINGTON, D.C. 20546

CONTRACT NASW-3314

JANUARY 1981

TRW
DEFENSE AND SPACE SYSTEMS GROUP

One Space Park, Redondo Beach, California

COMETARY PARTICULATE ANALYZER
DESIGN DEFINITION STUDY

FINAL REPORT

PREPARED FOR

NASA HEADQUARTERS
WASHINGTON, D.C. 20546

CONTRACT NASW-3314

JANUARY 1981

PREPARED BY:

N.G. UTTERBACK   (213) 536-1453

Principal Investigator: *N. G. Utterback*

N. G. Utterback

TRW
DEFENSE AND SPACE SYSTEMS GROUP

One Space Park, Redondo Beach, California

TABLE OF CONTENTS

FIGURES

FIGURES

SUMMARY

An experimental and analytical evaluation of a concept for determining remotely the relative abundance of elements contained in cometary particulates collected by a spacecraft has been conducted with very encouraging results. The technique utilizes a short ($\sim$ 10 ns) high intensity (10^9 - 10^{10} watts cm^{-2}) burst of laser radiation to vaporize and ionize collected particulate material. Ions extracted from this laser-produced plasma are analyzed in a time of flight mass spectrometer to yield an atomic mass spectrum representative of the relative abundance of elements in the particulates. Critical aspects in the development of this system are determining the ionization and collection efficiencies for the various atomic species combined in the particulates, and achieving adequate mass resolution. A literature survey revealed and experimental results indicate that the range of ionizing efficiencies is within acceptable bounds. The thermal energy spread within the high temperature plasma and velocity spread during acceleration tend to limit the mass resolution. However, a technique called energy-time focus utilizes static electric fields to alter the length of the ion flight path in proportion to the ion initial energy. This results in a corresponding compression in the range of ion flight times which greatly improves the inherent resolution.

During the present contract period, a prototype analyzer system was designed, constructed, and tested. The major accomplishments included the demonstration that energy-time focus does indeed perform as predicted in improving resolution, that power densities sufficient to produce usable ionization efficiencies can be obtained, that complex alloys such as stainless steel can be analyzed, and that a tiny, simple and reliable laser used in the demonstration easily meets spacecraft power and mass limitations. A mass resolution of 150 was experimentally demonstrated at mass 108, and an analytical extrapolation predicts a resolution sufficient to separate masses 250 and 251.

Areas requiring more work include increasing the sensitivity with more effective ion beam focus to minimize ion losses, decreasing the laser lens focal length to increase usable power density to minimize differences in species ionization efficiencies, and demonstrating the ability to make quantitative analyses of complex geological dust particles similar to the expected cometary particulates.

Sufficient data were acquired to develop preliminary specifications for a flight instrument. This instrument is unique in its ability to obtain at each shot a complete mass spectrum from mass 1 through mass 250 using 10^{-11} grams of material from a region defined within 10 micrometers, and in a measurement time of 10^{-4} seconds.

1.0 INTRODUCTION

This report summarizes the experimental and analytical work conducted under NASA Contract No. NASW-3314 for the period from 01 November 1979 to 31 January 1981. The overall objective of the program was to assess the feasibility of the Cometary Particulate Analyzer (CPA) concept for the in situ determination of the elemental composition of particulates released from a comet nucleus. Characterization of the physical and chemical properties of these particulates is one of the major scientific objectives of cometary rendezvous missions under consideration by NASA.

In the CPA concept, collected particulates are reduced to a high temperature plasma by irradiation with a short pulse of high intensity laser light. Ions are extracted from the plasma by application of an electric field at the particulate collector surface. The extracted ions are accelerated by the same electric field to a fixed kinetic energy and are subsequently analyzed in a time of flight ion mass spectrometer. The raw data from the CPA gives the relative number of ions as a function of atomic weight. In principle, the accelerated ion stream contains ions of all of the elemental species present in the particle including normally volatile fractions. The degree of ionization of a given atomic species depends upon its ionization potential and the temperature of the plasma. In practice, the plasma temperature must be high enough to ionize a significant fraction of the high ionization potential atomic species expected to be present in the particulates. At these temperatures, the number of molecular ions present in the plasma is expected to be vanishingly small. We expect that it will be possible to determine the relative abundance of all of the significant elements contained in the particle. Given the relative elemental abundances, it may be possible to reconstruct the mineralogical structure of the particulates.

The combination of laser blow-off ionization and time of flight (TOF) mass spectrometry that comprises the CPA was arrived at after careful consideration of other techniques for accomplishing either or both of the

necessary functions. We believe for a variety of reasons, some fundamental and some practical, that the CPA is a strong candidate for the eventual flight experiment. Based partially on our work and partially on the work of others as reported in the literature, we believe that the CPA is potentially capable of unambiguously specifying the relative abundances of all elements (including condensed volatile material) contained in the collected particles over the atomic mass range from 1 to 250 amu. The arguments in support of this belief are delineated in the balance of this report.

The following subsection describes briefly the end scientific objectives for the project. Section 2 describes the CPA concept for the purpose of identifying the critical issues that must be resolved in order to establish the feasibility of the approach. Section 3 describes the present experimental apparatus and results of measurements conducted under a previous program and summarizes their significance. In Section 4 we describe the concept of "energy-time focus" which is a technique for improving the mass resolution of the CPA. The requirement for energy-time focus will become clear in the discussion preceding its description. Section 5 contains our current results and a discussion of necessary future improvements and experiments. Section 6 presents our best estimate of some of the specifications of a flight experiment that will yield the results described above.

1.1 SCIENTIFIC OBJECTIVE

This section draws freely on the NASA Comet Science Working Group Report, November 1979 (CSWG Report).

"A major objective of NASA's program of space exploration is to deepen man's understanding of the origin and evolution of his cosmic environment. The past decade has witnessed the initial stages of a spectacularly successful program of planetary exploration. However, planets and their satellites retain at best a blurred record of their births, obscured by billions of years of evolution during which complex processes have reshaped their interiors and surfaces. By contrast, comets

2

are among the most primitive objects remaining in our solar system.
Because of their minute size and the fact that they have spent most of
their existence deep-frozen on the fringes of the solar system, comets are
expected to preserve the chemical and physical characteristics with which
they were formed.

The nucleus is the source of all cometary material. Appropriately,
the first goal of the comet mission is to determine the chemical nature
and physical structure of the constituents of cometary nuclei. In order to
understand the cometary nucleus, its constituents and their interactions
with the interplanetary medium, a wide variety of data is needed (Table 2-5
CWSG Report Nov. 1979). Some of these goals can be met only by combining
results of a variety of measurement. The Subgroup (on dust and solids,
CSWG) felt it must define a limited subset of goals which, if met, would
permit a reliable, first-order deduction of what are the solid (ices and
dust) constituents of the nucleus. These more limited objectives are to
determine:

(1) The elemental composition of collected solids (dust and icy
     particles).

(2) The flux and physical characteristics such as size, shape,
     velocity, charge, scattering properties, etc., of dust and icy
     particles.

These data, combined with those derived from other measurements
(imaging, remote analysis, mass spectrometry, etc.), will provide the
means of addressing most of the goals listed. The subgroup concluded
that a necessary step to achieving an understanding of the nucleus is to
determine the chemical composition of the solids emitted by the comet.
Although, ideally, the absolute abundances of all the elements present in
cometary material should be determined, this goal is not realistic. By
selecting "indicator" elements, each of which is representative of a group
of elements in terms of their cosmochemical behavior, measurement of
12-15 elements in the nucleus and dust can yield a rather complete picture
of the overall composition of the nucleus. Table 2-6 (CSWG, reproduced

3

as Table 1.1) is a prioritized list of elements selected for this purpose.
Instruments for the measurement of elemental composition of the nucleus and
the dust should be selected, in large part, on the basis of their ability
to measure elements in the first two categories on the list. We note that
several instruments exist which come reasonably close to achieving this
goal. A secondary consideration is the amount of dust required for
measurement; the smaller the sample required, the more desirable is the
instrument.

The instruments should be capable of determining compositions which
differ substantially from those expected. The capability of measuring a
large number of diverse elements accurately is the best assurance that a
reliable determination of the elemental composition of the collected dust
will be achieved."

It is asserted that the Laser Blow-off Cometary Particulate Analyzer
described here is an excellent candidate to be one of the instruments
to carry out these scientific objectives as set forth by the CSWG report.

1.2 Anticipated Scientific Results

The Laser Blow-off Cometary Particulate Analyzer is expected to
provide mass spectra with better than unit resolution from mass 1 to
mass 250 from a 10 µm diameter region 1 µm deep at each laser shot, and
in a time of 10^{-4} seconds. An example of such a spectrum is presented
as Figure 1.1, obtained with a commercial instrument using the identical
concept (Leybold-Heraeus, Inc. LAMMA) and reproduced from Industrial
Research and Development, April 1979.

When compared with spectra from standards of similar and known elemental
content, such spectra from cometary particulates should facilitate the
determination of their elemental content for a wide range of species and
concentration. A comprehensive determination of the relative ionization
and collection efficiencies for various atomic species will be necessary to
determine possible variations due to complex specimen matrices.

By varying the laser energy, it may also be possible to obtain some
information regarding the molecular structure of the samples since at lower
temperatures incomplete dissociation would be expected.

4

Table 1.1 Measurement Priorities for Bulk Analysis of the Nucleus
and Collected Cometary Solids[a]

Rating	Element/Si	ΔR[b]	R in Chondrites
Highest priority	Mg	± 0.05	0.7 - 1
	Ni	± 0.02	0.04 - 0.1
	S	± 0.05	0.1 - 0.7
	H	± 0.03	0 - 0.2
Essential (listed in order of descreasing priority)	Fe	± 0.2	1 - 2
	C	± 0.05	0 - 0.5
	O	± 0.3	1.5 - 5
	Na	± 0.005	0.03 - 0.06
	Al	± 0.01	0.05 - 0.12
	K	$\pm 10^{-3}$	$2-10 \times 10^{-3}$
	Ca	± 0.01	0.06 - 0.14
	Zn	$\pm 10^{-4}$	$1-30 \times 10^{-4}$
	N	± 0.01	$1-200 \times 10^{-4}$
	Mn	± 0.001	0.01 - 0.02.
	U	$\pm 5 \times 10^{-8}$	$4-20 \times 10^{-8}$
	P	± 0.001	$4-20 \times 10^{-3}$
Desirable (Not prioritized, listed in order of increasing atomic number)	Li	$\pm 10^{-6}$	$4-15 \times 10^{-6}$
	Ne	$\pm 5 \times 10^{-9}$	$0 - 3 \times 10^{-8}$
	Cl	$\pm 10^{-4}$	$4-600 \times 10^{-5}$
	Ar	$\pm 5 \times 10^{-9}$	$1 - 20 \times 10^{-9}$
	Ti	± 0.001	$2-10 \times 10^{-3}$
	Cr	± 0.002	0.02 - 0.03
	Ge	$\pm 10^{-5}$	$6 - 40 \times 10^{-5}$
	Ce	$\pm 2 \times 10^{-6}$	$\sim 6 \times 10^{-6}$
	Xe	$\pm 5 \times 10^{-10}$	$2 - 20 \times 10^{-10}$
	Yb	$\pm 3 \times 10^{-7}$	$\sim 10^{-6}$
	Tl	$\pm 10^{-7}$	$3-1000 \times 10^{-9}$
	Pb	$\pm 10^{-5}$	$1-30 \times 10^{-6}$
	Th	$\pm 2 \times 10^{-7}$	$2-10 \times 10^{-7}$

[a]Weight ratios normalized to Si, R = element (weight fraction)/Si
(weight fraction).

[b]The ΔR's are chosen to permit various meteoritic classes to be
distinguished from each other and from non-meteoritic material.

Spectrum obtained
from NBS glass
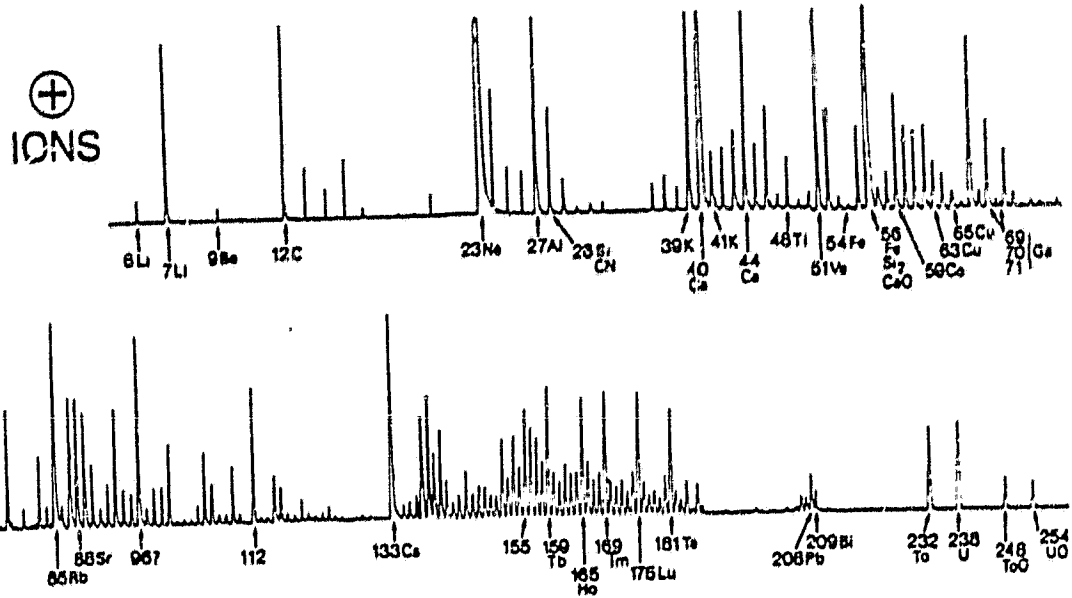standard material 611
Analyzed volume is
about 10^{-13} g

Figure 1.1   Mass Spectrum (Reproduced from "Industrial Research
and Development" April 1979)

6

2. CPA CONCEPTUAL DESCRIPTION

2.1 PRINCIPLES OF OPERATION

Figure 2-1 is a sketch of the simplest CPA configuration. The particles to be analyzed are assumed to be at rest on the surface of a collector that has been retracted from a region exposed to the particulate flux to the position indicated in the sketch. (Implementation of the required manipulation of the collector, its geometric form, and the material from which the collector is fabricated were not evaluated in any detail during the course of this study.) The collector is maintained at a positive potential relative to spacecraft ground by a low-current power supply. A grounded planar grid mounted parallel to the collector surface and a distance L_1 from it establishes an electric field between the collector and the grid.

Irradiation of the collector surface with a focused, high intensity burst of laser light converts a thin layer of the material within the laser spot into a highly ionized plasma. Due to high internal pressure, the plasma bubble begins to expand into the surrounding vacuum. As the plasma density begins to drop because of the expansion process, the applied electric field extracts ions from the plasma and accelerates them across the gap between the collector and the grounded grid.

Neglecting for the moment any thermal velocity derived from the hot plasma, the velocity of an ion upon reaching the plane of the grid is

$$v = \left(\frac{2qV}{m}\right)^{1/2} \text{ m sec}^{-1} \tag{2.1}$$

where V is the voltage difference between the collector plate and the grid and q/m is the charge to mass ratio of the ion. Upon passing through the grid, the ions enter a field free region where they drift at constant velocity to an ion detector located at a distance L_2 from the accelerator grid. The time interval required for an ion to traverse the distance from the collector to the ion detector is given by

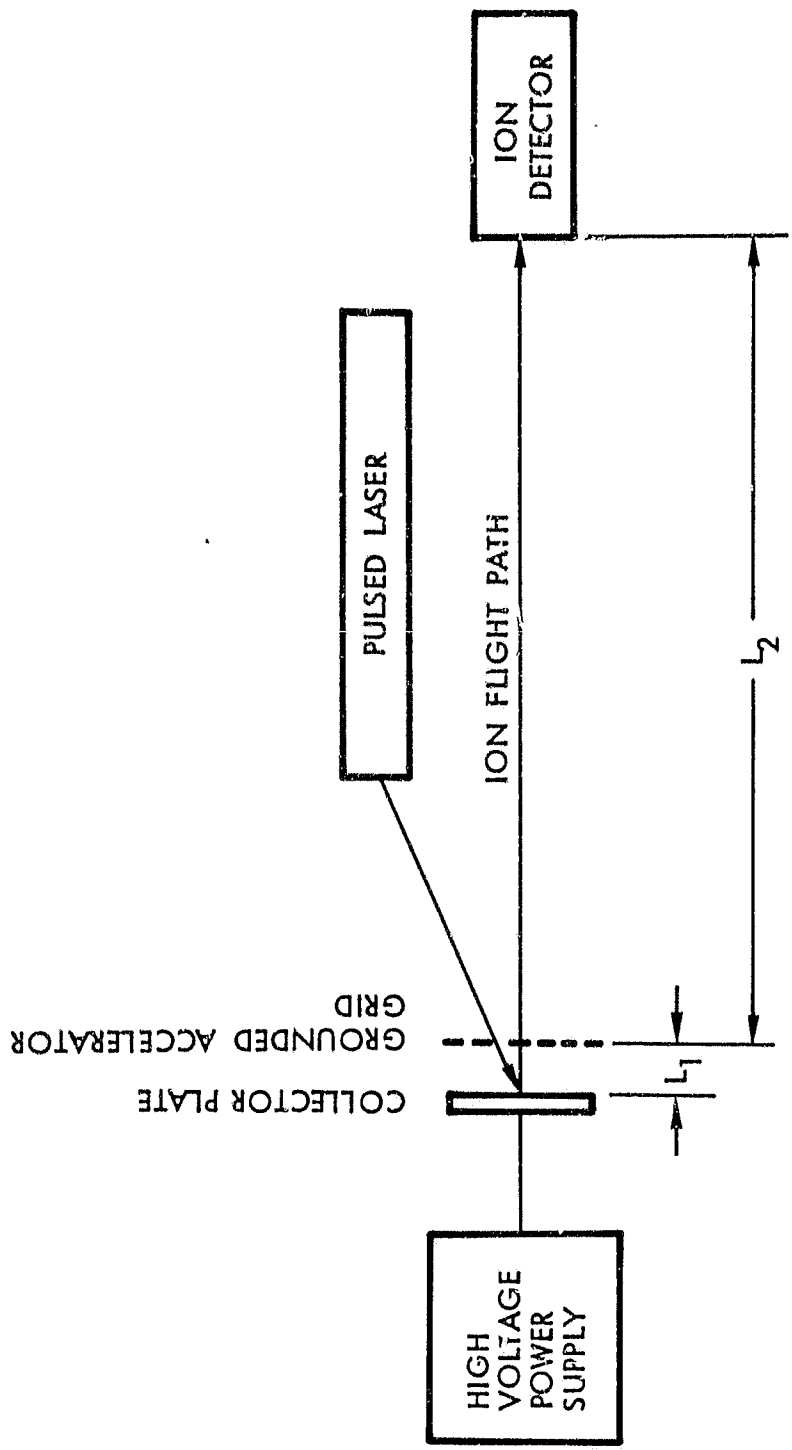$$t = L\left(\frac{m}{2qV}\right)^{1/2} \text{ sec} \tag{2.2}$$

Figure 2-1. Conceptual Cometary Particulate Analyzer.

where $L = 2L_1 + L_2$. The difference in arrival times of two ion groups with atomic masses m_1 and m_2 with $m_2 > m_1$ is given by

$$\Delta t = \frac{L}{V^{1/2}} \left(0.72 \times 10^{-4}\right)\left(m_2^{1/2} - m_1^{1/2}\right) \text{ sec} \qquad (2.3)$$

where MKS units have been assumed.

Thus, this approach segregates the various mass ions by their arrival time at the detector. A recording of the time-dependent ion current yields a mass spectrum of the plasma ions where the relative magnitude of the ion current peaks is related to the relative abundance of ions in the plasma.

This idealized description of the CPA serves to identify some of the reasons for choosing this particular approach to the analysis of cometary particles, specifically;

1. The output signal for a given "event" includes the entire atomic mass range of interest.

2. Weight and power demands are minimal, requiring only a low average current high voltage supply and a long enough drift distance to yield the desired resolution.

3. The system requires only a single ion detector and associated. electronics.

2.2 FACTORS AFFECTING CPA PERFORMANCE

2.2.1 Atomic Mass Resolution

Equation 2.2 shows that there is a unique relationship between the charge to mass ratio of an ion and its transit time through the time-of-flight range. In practice, however, several effects combine to produce a smearing in the arrival time at the ion detector. This causes a finite width of the ion pulses and has the potential of degrading the effective resolution of the instrument. The resolution may be defined as the ratio of the mean time of arrival of a group of ions with a given charge-to-mass to the time width of the ion pulse. For the idealized case discussed above, the pulse width is zero and the resolution infinite.

One of the factors contributing to a finite pulse width is the time interval over which ions are extracted from the plasma. This time interval

will likely be on the order of the laser pulse duration. If this is the case, the difference in the arrival times of two ion groups must be greater than the laser pulse duration for the two ion groups to be resolved, i.e., $t_L \leq \Delta t$ where t_L is the laser pulse duration. Utilizing this relationship in Equation 2.3 yields an upper limit for the accelerating voltage given by

$$V_{max} \leq \left(\frac{L}{t_L}\right)^2 0.518 \times 10^{-8} \left(m_2^{1/2} - m_1^{1/2}\right)^2 \text{ volts} \quad . \quad (2.4)$$

Figure 2-2 gives the maximum accelerating voltage as a function of m_2 for two values of t_L. Here we have arbitrarily chosen L = 0.5 meter and have defined $m_1 = m_2 - 1$ meaning that the indicated voltage for a given value of m_2 results in resolution of the m_1 and m_2 ion peaks.

Another factor that may affect the width of the ion pulses is the time interval over which ions are extracted from the plasma even if the time required to form the plasma is small. Efficient extraction can occur only when the applied electric field dominates the space charge forces tending to maintain charge neutrality. If we treat the accelerator region as a planar diode with ions extracted from the heated spot on the anode, the space charge limited ion current density is given by the expression

$$J_+ = \frac{\varepsilon_0}{2.25} \left(\frac{2q}{m}\right)^{1/2} \frac{V^{3/2}}{L_1^2} \text{ amps cm}^{-2} \quad (2.5)$$

where ε_0 is the permittivity of free space. For singly charged silicon ions, for example, the maximum current density is

$$J_{Si+} = 1.03 \times 10^{-8} \frac{V^{3/2}}{L_1^2} \text{ amps cm}^{-2} \quad . \quad (2.6)$$

For illustrative purposes, assumed values of V = 2000 volts and L_1 = 1 cm gives a maximum Si ion current density of 0.92×10^{-3} amps cm^{-2}. For a laser spot size of 0.03 cm diameter, the total current that can be transported across the diode is 6.5×10^{-7} amperes. For a time interval of 50 nsec, the total charge that can be transported is 3.25×10^{-14} coulombs.

Although these assumed conditions are somewhat unrealistic, the calculations convincingly illustrate the importance of space charge forces
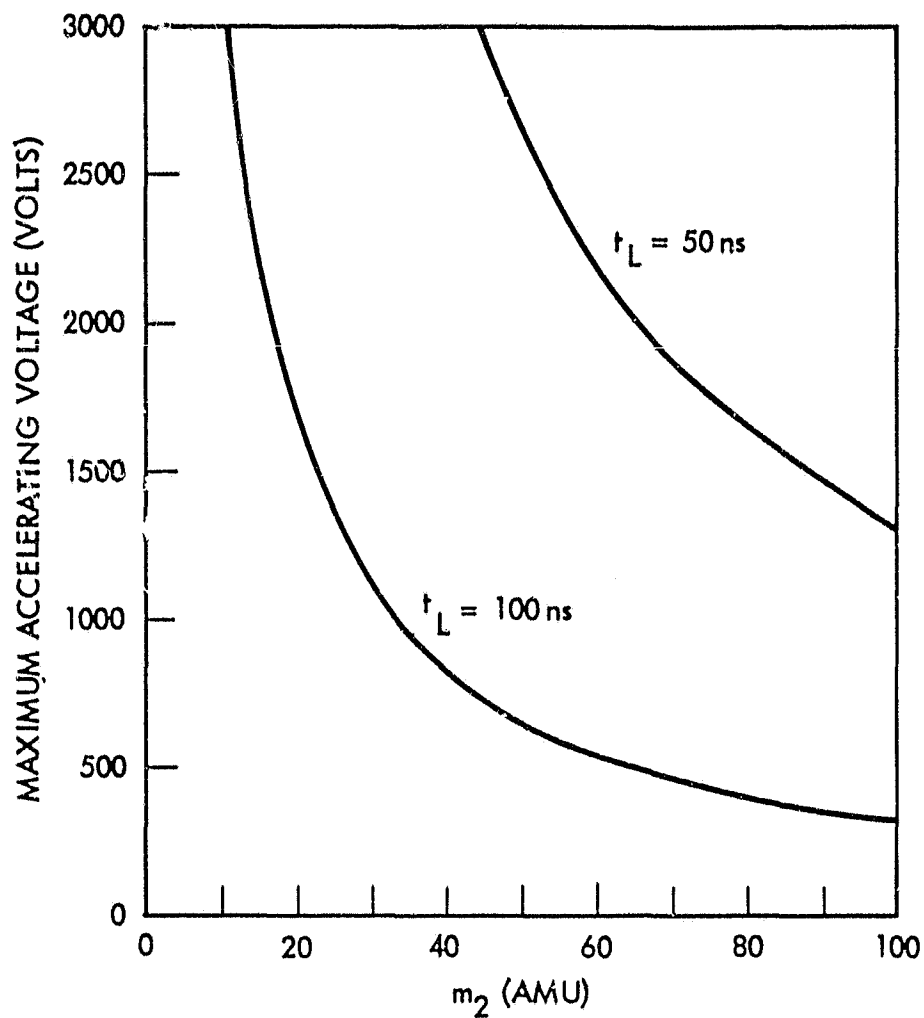
10

Figure 2.2. Maximum accelerating voltage resulting in
resolution of the ion peaks corresponding to
masses m_2 and m_2-1 for two values of laser
pulse duration. A TOF distance of 0.5 M was
chosen.

11

on charge extraction from the plasma. Further, they show that the total amount of charge produced by the laser bombardment has an upper limit. In practice, values of the current density, total ion current, and integrated charge are probably lower limits due to the dynamic nature of the plasma. Some degree of radial expansion of the ions can be tolerated which has the effect of increasing the area of the diode. The plasma can expand into the diode space effectively decreasing the diode separation. Finally, ions within the plasma have a finite thermal energy. All of these factors combine to increase the ion current that can be extracted from the plasma and transported across the space. Experiments conducted during this program have shown that satisfactory conditions can be achieved. The experiments have also shown that the production of excess ionization does affect the resolution and, in extreme cases, the plasma can penetrate to the grid causing an arc to form across the accelerating region.

Another factor that contributes to broadening of the individual ion peaks is the variation in initial energy of the ions. Equation 2.2 tacitly assumes that $v_0 = 0$. More realistically there will be a range of initial velocities in the plasma due to the high plasma temperature. The range encompasses zero at one extreme and some sensible upper limit where the fraction of ions with velocities in excess of the upper limit is small enough to be ignored. The drift velocity of an ion with an initial energy E_0 after acceleration through a potential difference V is

$$v = \left[\frac{2}{m} (E_0 + qV)\right]^{1/2} \text{ m sec}^{-1} \quad . \tag{2.7}$$

The transit time to the detector in the time of flight range is given by

$$t = \frac{L}{\left[\frac{2q}{m} V (1 + k)\right]^{1/2}} \text{ sec} \tag{2.8}$$

where $L = 2L_1 + L_2$ as before and it is assumed that $L_1 << L_2$. Also, in Equation 2.8, the initial energy has been given as a fraction of the energy imparted to the ion by the applied electric field, i.e. $E_0 = kqV$. For illustrative purposes, let us consider the effect on the arrival time of two ion groups of masses m_2 and m_1 with $m_2 > m_1$ when a range of initial

velocities exists. Ignoring the effect of a finite pulse duration, the _latest_ arriving ions with mass m_1 are those with zero initial energy. The _earliest_ arriving ions with mass m_2 are those with the maximum initial kinetic energy. In order to resolve the two groups we require that the latest time of arrival of the mass m_1 ions be _less_ _than_ the transit time of the fastest mass m_2 ion, i.e.

$$\left[\frac{L}{\frac{2qV}{m_1}} \right]^{1/2} \leq \left[\frac{L}{\frac{2qV}{m_2}(1+k)} \right]^{1/2} \quad . \qquad (2.9)$$

Solving for k from Equation 2.9 yields the result

$$k \leq \frac{m_2}{m_1} - 1 \quad . \qquad (2.10)$$

In other words, the energy gained through the electrical acceleration of the ions has to be larger than the "sensible" maximum initial energy by a factor of at least 1/k to result in resolution of the two ion peaks. Figure 2-3 presents a family of curves giving the minimum acceleration voltage as a function of m_2 for several assumed values of E_0. As in our previous example we have taken $m_1 = m_2 - 1$ meaning that an accelerating voltage greater than the value read off one of the curves at a given value of m_2 results in the resolution of the adjacent m_1 and m_2 ion peaks.

Of the factors considered above, those resulting in a finite pulse width at the accelerator grid (i.e. finite laser pulse length) tend to establish an upper limit to the accelerating voltage while the finite energy spread sets a lower limit to the accelerating voltage. Figure 2-4 is a composite of Figures 2-2 and 2-3 for "reasonable" values of t_L = 50 ns and E_0 = 20 eV showing that there is a large range of accelerating voltage that provides adequate resolution of the interesting part of the atomic mass range. In the example, all of the area to the left of the shaded area would result in satisfactory resolution.

The purpose of the foregoing discussion was to provide a context for the experiments discussed in Section 3. A more comprehensive model of the ion extraction and acceleration processes that combines the various factors is described in Section 4.
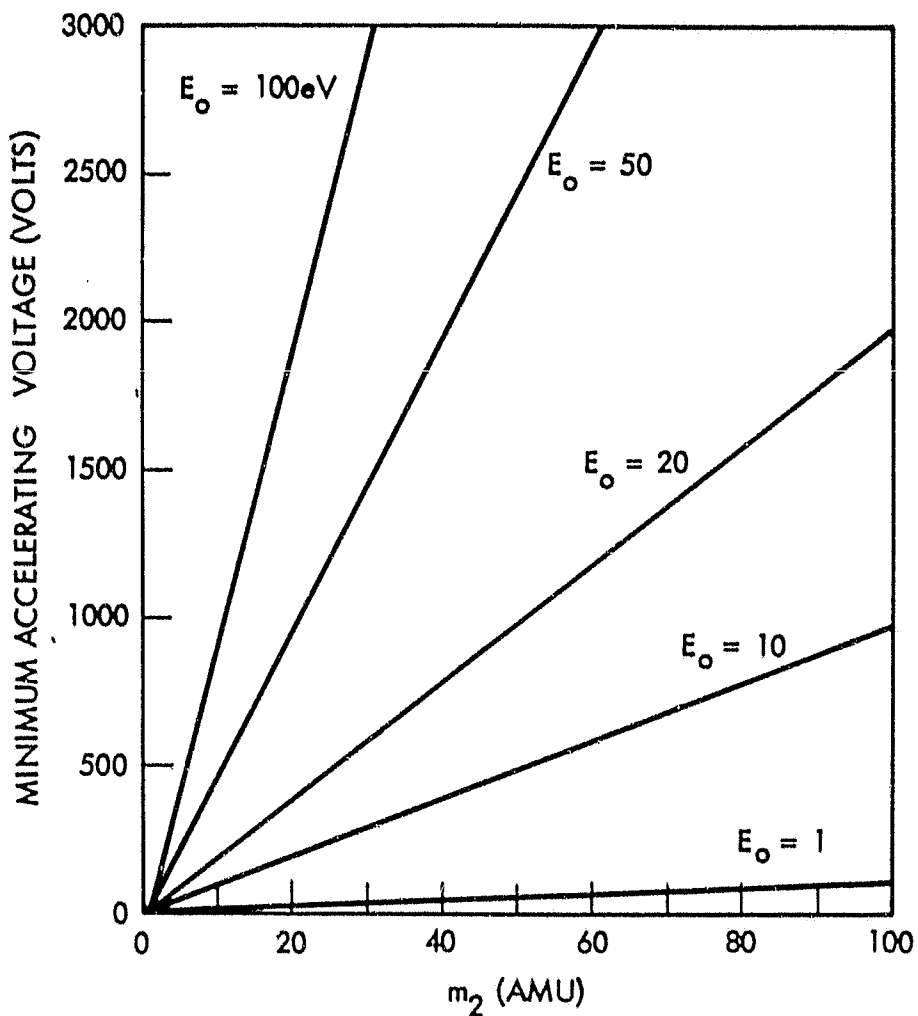
13

Figure 2-3. Minimum accelerating voltage required to give equal final velocities for ions with masses m_2 and m_2-1 for a range of initial energies of the heavier ion. The lighter ion is assumed to have zero initial energy.
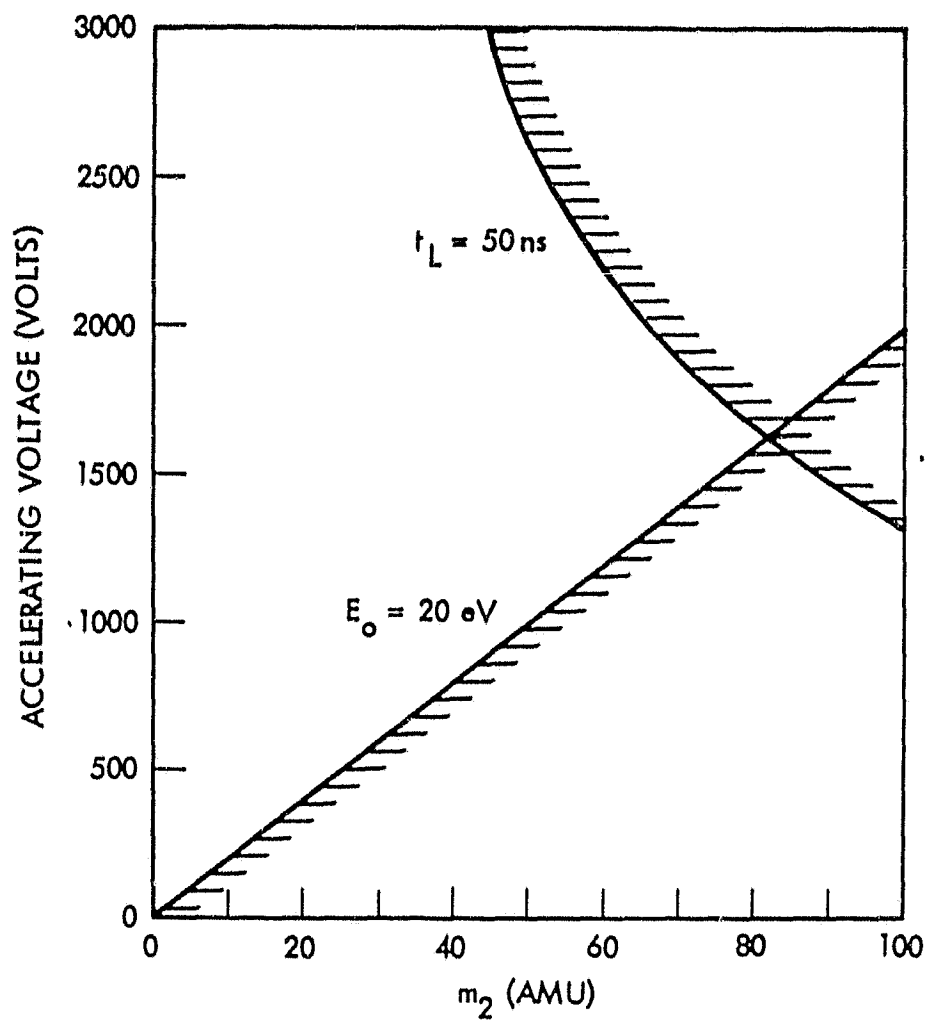
14

Figure 2-4. Composite of Figures 2-3 and 2-4 that defines the acceptable accelerating voltage range with the two conflicting requirements.

15

2.2.2 Ionization Efficiency

When a plasma in thermal equilibrium at absolute temperature T contains several species of atoms and ions, the degree of ionization of each species s whose ionization energy is E_{I_s} is related to T according to Saha's equation

$$n_e n_{i^s}/n_{n^s} = CT^{3/2} U_{i,n^s} \exp\left(- E_{I_s}/kT\right) \tag{2.11}$$

where n_e, n_{i^s}, and n_{n^s} are the numbers per unit volume of electrons, ions of species s, and neutral atoms of species s, respectively; C is a constant; $u_{i \cdot n^s}$ is the ratio u_{i^s}/u_{n^s}, in which u_{i^s} and u_{n^s} are respectively the internal partition functions of ions and neutrals of species s; and k is Boltzmann's constant. The Saha equation shows that the fractional ionization of a given species of atom depends on the ratio of the ionization energy of that species to the mean thermal energy of the plasma.

For a plasma containing only two atomic species, Eq. 2.11 can be written for each of the two species. Dividing one of these expressions by the other yields

$$\frac{n_i^{(1)}}{n_n^{(1)}} = \frac{n_i^{(2)}}{n_n^{(2)}} f(T) \exp\left[\left(E_I^{(2)} - E_I^{(1)}\right)/kT\right] \tag{2.12}$$

where $f(T) = u_{i,n}^{(1)}/U_{i,n}^{(2)}$. $f(T)$ is a slowly varying function of T compared to the exponential term. Equation 2.12 shows that for nearly equal ionization potentials of the two species, the fractional ionization of the two species is nearly equal at all temperatures and the relative number of atoms of the two species can be determined by measurement of the relative number of ions. For atomic species with widely differing ionization potentials, the relative degree of ionization of the two species is strongly dependent upon T at low temperatures but the relative degrees of ionization asymptote to the same value in the limit of $kT \gg (E_I^{(2)} - E_i^{(1)})$. This argument can be readily extended to a plasma containing several atomic species.

We would not argue that the Saha equation describes the laser blow-off phenomenon because of the rapidly varying conditions within the plasma. Furthermore, Eq. 2.12 is really only valid for weakly ionized plasmas and it doesn't consider the dissociation of molecular species nor the multiple ionization of atomic species. It is fairly obvious, however, both from intuitive arguments and from the results of experiments discussed elsewhere in this report, that a high plasma temperature is required to approach comparable ionizing efficiencies for the plasma constituents. In practice, it will probably be possible to make a reasonably good estimate of the ionizing efficiency for all of the ionic species in the spectrum.

The requirement for high plasma temperature to achieve reasonably uniform ionization efficiencies results in a fairly broad initial ion energy range which, as noted above, tends to degrade the resolution of the CPA. However, the energy focus technique described in Section 4 provides a solution to this problem.

2.3 Factors Affecting Validity of CPA Data

The unambiguous analysis of cometary material collected by a remote probe as to chemical composition and structure is a major technological challenge. Almost without question several analytical techniques which complement each other will be necessary. Since weight and power considerations severely limit the number and type of instruments which can be carried, it will be necessary to choose an optimum array of instruments. It is the purpose of this discussion to describe one type of instrument which we believe would supply very valuable capabilities to a cometary rendezvous probe.

The instrument and technique may be characterized as a "Laser Blowoff Mass Analyzer" (LABMA). In simplest terms the instrument is an ion mass spectrometer whose source of ions consists of a tiny expanding plasma "bubble" of material to be analyzed, produced through vaporization and ionization of a very small volume of the material by a pulsed laser beam focused onto the material. In a generic sense only the ion source is unique to LABMA and in principle it could be attached to any type of ion mass spectrometer. However the inherent very short pulsed nature of the ion source lends itself well to time-of-flight mass analysis with its clear advantage of being almost passive without DC magnetic fields or RF electric fields. For example no source of RF power is needed as with a quadrupole mass spectrometer, and no RF background is produced; no stray DC magnetic fields are produced as with a magnetic deflection mass spectrometer. Furthermore, no "sweeping" over the mass range is necessary since an entire mass spectrum is collected with each laser shot. (It may be noted that these features contrast with Secondary Ion Mass Spectrometry, SIMS, which precludes use of time-of-flight mass spectrometers.) Because of these advantages of the time-of-flight (TOF) mass analyzer, and because

TOF appears to be feasible in conjunction with LABMA, this discussion will assume that LABMA will utilize TOF mass analysis

The key element in the LABMA method is the production of ions through deposition of laser energy in the sample to be analyzed, causing rapid vaporization and ionization of sample material. The process is very complex and a number of questions about this ion source must be considered.

1. Most importantly, is the ratio of the number of ions produced to the number of atoms in the sample the same for all atomic species regardless of chemical structure?

2. What is the charge state of the ions (single or multiple charge), and to what extent does it depend on species?

3. What is the chemical state of the ions (atomic or molecular), and how does it depend on the chemical structure of the original sample?

4. What is the kinetic energy of the ions as they enter the mass spectrometer?

5. How many ions are produced per laser pulse?

6. What is the time dependence of the ion pulse?

As would be expected the answers to these questions depend on the degree of quantitative accuracy demanded for the measurements. The discussion following will attempt to give reasonable answers. The first three are basic to the analysis method by LABMA, while the latter three are related to the resolution and sensitivity of the TOF mass spectrometer. It is asserted here that for the main atomic species of interest, sufficient evidence will be presented to strongly suggest that useful data can be obtained from LABMA analyses on samples of unknown character, and if it is possible to calibrate with samples resembling the actual cometary particulates to be encountered, results with good accuracy ($\pm$ 20%) should be obtainable. It must be emphasized however that only with thorough studies of a variety of materials with an actual operating LABMA can such a suggestion be validated.

On the other hand, of the analytical methods utilizing a mass spectrometer, which would be essential to obtaining isotopic ratios (e.g. SIMS),

the LABMA source of ions appears least subject to errors due to these questions. A considerable literature[*] is available which points out the large ($\times 10^3$) differences in sensitivity as a function of species and chemical composition encountered in SIMS analyses, as well as the positive attributes of SIMS for certain types of measurements. By contrast, it has been reported by several investigators[+],[#] that LABMA-type laser blow-off ion sources are relatively less subject to differences in ionization efficiencies between chemical species, particularly so for metals (to less than $\times 2$).

1. Thus with regard to Question 1 concerning overall detection efficiency for various species, the extensive work[+] of a German group is valuable. In conjunction with the company Leybold-Heraeus they have developed a Laser Microprobe Mass Analyzer, LAMMA. (It is also a LABMA by our definition). Their LAMMA is designed to laser vaporize, ionize and time-of-flight mass analyze sub-cellular volumes 0.5 μm dia x 0.5 μm thick of biological tissues in order to map species location within cells. The instrument is commercially available and proves the feasibility of a LABMA with high resolution (both mass and spatial), high sensitivity, and calibratable detection efficiency even for biological specimens. Cometary particulate analysis, with a less complex species makeup, should be less demanding. See Figure 1.1.

---

[*]   W.H. Christie, D.H. Smith, R.E. Eby and J.A. Carter, International Laboratory July/August 1978, International Scientific Communications, Inc., Fairfield, CT 06430.

A. Benninghoven, Appl. Phys. 1, 3 (1973)

A. Benninghoven, Z. Physik 220, 159 (1969)

H.E. Beske, Z. Naturforsch 22a, 459 (1967)

[+]   F. Hillenkamp, E. Unsöld, R. Kaufmann and R. Nitsche, Appl. Phys. 8, 341 (1975).

R. Wechsung, F. Hillenkamp, R. Kaufmann, R. Nitsche, H. Vogt, 1979 Conference Scanning Electron Microscopy, Los Angeles, April 17-21, 1978

[#]   J.F. Eloy, Int. J. Mass Spectrom. Ion Phys. 6, 101 (1971)

N.C. Fenner and N.R. Daly, Rev. Sci. Instr. 37, 1068 (1966)

The preceding Reference[+] lists ionization sensitivities for a number of metals in small concentration in organic films. Except for the alkali metals which have an order of magnitude higher sensitivity, the sensitivities for a variety of metals vary by a factor of x30 for the Leybold-Heraeus LAMMA configuration. However, the LAMMA configuration is probably not the optimal LABMA for the cometary particulate analyzer for several reasons. First, the laser beam strikes the backside of what is essentially a free standing very thin film; thus "large" (greater than tens of microns thickness) cometary particulates could not be reliably analyzed. Second, it appears that plasma temperatures are low enough to cause the ionization sensitivities to vary markedly because of different ionization potentials; this is probably also due to the "backside" illumination. The appearance of both positive and negative ions, as well as molecular ions, gives a measure of the temperatures reached in the LAMMA configuration. There is one great advantage to this LAMMA configuration, in that it produces ions with very low (few eV) initial energies (as well as being essential for simultaneous microscopic observation and sampling of biological samples for which it is designed). Low initial energies are essential to adequate mass resolution for TOF mass spectrometers of reasonable size, unless an "energy-time focus" is utilized. Such an energy-time focus technique has been discovered, and it will be described later in this paper. It is being used by both the LAMMA group and us. If it is assumed for the moment that initial ion kinetic energy is unimportant, a more appropriate LABMA ion source may be discussed which appears from published data to be almost ideal for cometary particulate analysis. Eloy (preceding Reference #) describes such a device which utilizes front-surface illumination, 200 nsec ruby laser pulse, 5 mJ pulses, 200 μm dia spot, 0.6 μm depth, and achieves quantitative ($\pm$ 20%) analysis of metals from a variety of alloys and minerals. Although the pulse length is somewhat too long for TOF and the spot size is a bit larger than desired, these parameters are close enough to those desired to suggest that results will still be good with the better parameter values. This must obviously be tested. Eloy was not concerned with initial ion energies since he overwhelmed the initial energy effects with acceleration to high energies followed by magnetic mass analysis and photographic plate detection.

The results of Eloy (and less extensive results of our own) suggest that front surface illumination produces higher temperatures on the leading edge of the plasma bubble and therefore, less variation in ionization efficiencies caused by differing ionization potentials, and that quantitative mineral analysis is achievable so long as initial ion energy may be neglected. This initial energy aspect will be discussed further below. Our results at this point in the development are similar to those of the LAMMA group.

2. The question of the charge state of the ions does not appear to pose major problems, based on the work of the LAMMA group and Eloy, and our present results. The former speak of doubly charged ions being less than 10^{-3} abundant, while Eloy speaks of "very small amounts", even at the apparently higher temperatures from front surface illumination. The LAMMA group report seeing halogens only as negative ions, while Eloy does not mention negative ions. We have seen no signs of multiply-charged ions from our front surface illumination results.

3. The chemical state of the ions (molecular or atomic) appears to depend on whether front or backside illumination is used. Thus Eloy with frontside illumination, higher temperatures and less dependence on ionization potentials reports no molecular ions. The LAMMA group report organic "fingerprints" of series of organic molecular ions, but indicate the results are very sensitive to laser illumination conditions. If front surface illumination is used, it appears likely that only atomic ions will be significant, and therefore no chemical structure analysis will be possible. On the other hand, reducing the laser power density might give at least qualitative data on molecules, and this should certainly be tested. We have observed small amount of molecular species.

4. The question of initial ion kinetic energy is critical if TOF (time of flight) mass analysis is to be used. The LAMMA group reports initial energies of a few eV for the backside illumination or organic films, but energies far above 100eV for metal films. Other groups (Fenner, preceding Reference #) report initial energies to above 200 eV. Eloy reports no measurement of initial energies, but by comparing his mass spectra using the LABMA-type source versus a spark source, it is possible to infer that his initial energies were up to 100 eV, and appeared

22

to have a roughly Maxwell-Boltzman distribution with kT = 50 eV. Although prohibitively high for a conventional TOF mass spectrometer, this initial energy (or even x 4 higher) can be easily handled by the energy-time focus TOF to be described below. Thus it appears that from the standpoint of initial ion energy, a front surface illumination LABMA is feasible. Our present results corroborate this.

5. The number of ions produced per pulse in the Eloy experiments was 2×10^{11} ions total per pulse, with about 1/6 of these passing through the spectrometer. Actually the problem is too many ions when the energy time focus technique is applied due to space charge problems. At worst, if space charge is a problem, multiple laser shots at lower ion production per shot could be necessitated. It certainly appears that sufficient ions will be produced per laser shot to analyze the major expected species from cometary particulates. Our results indicate an upper limit on usable ion numbers per shot of 10^7.

6. In order to use TOF (time-of-flight) mass analysis, it is necessary to have all ions produced in a time short compared to the difference in ion flight times between the highest adjacent mass peaks of interest. For the TOF to be described and for mass resolution of 100, maximum allowable ion production times are around 30 nanoseconds. This is easily obtainable with Q-switched lasers which deposit their energy in 10 to 50 nanoseconds. This is consistent with laser pulse lengths used for LAMMA and earlier work, but is shorter than Eloy (200 nanoseconds). Although it is expected that shorter pulse lengths would not have changed Eloy's results appreciably, this must be tested. Our present apparatus employs 10 nanosecond pulses.

3. EXPERIMENTAL MEASUREMENTS

3.1 EXPERIMENTAL APPARATUS

Figure 3.1 is a picture of the external experimental apparatus, showing the vacuum enclosure, vacuum pumps and power supplies. The knobs on the enclosure remotely position various elements within the vacuum, such as the laser beam focal point position, lateral target spot position, reflection region angle and detector position. The large enclosure size was chosen for convenience in varying the CPA configuration in obtaining an eventual optimal flight design.

Figure 3.2 is a picture of the internal apparatus, showing the elements associated with the laser beam and ion beam flight paths, looking from the laser target (sample) along the ion beam path toward the reflection region. The entrance and exit apertures to and from the reflection region are visible (exit partially covered). The laser beam enters from the left, crosses to the mirror and is reflected through the lens to focus on the circular target holder. Acceleration takes place between the target and the square electrode plate 1 cm away.

Figure 3.3 shows the internal apparatus viewed against the ion beam direction and toward the target. The laser beam enters from the right and crosses to the mirror and reflects through the lens, focusing at 30° from normal on the target. Clearly visible in this picture are the guard rings producing the uniform field in the reflection region, and the ion-electron multiplier detector at the ion exit. The reflection region has 25 rings spaced 1 cm apart. The laser and beam expander are under the white cover to the right of the enclosure.

Figure 3.4 is a schematic diagram of the experimental layout. It is self-explanatory.
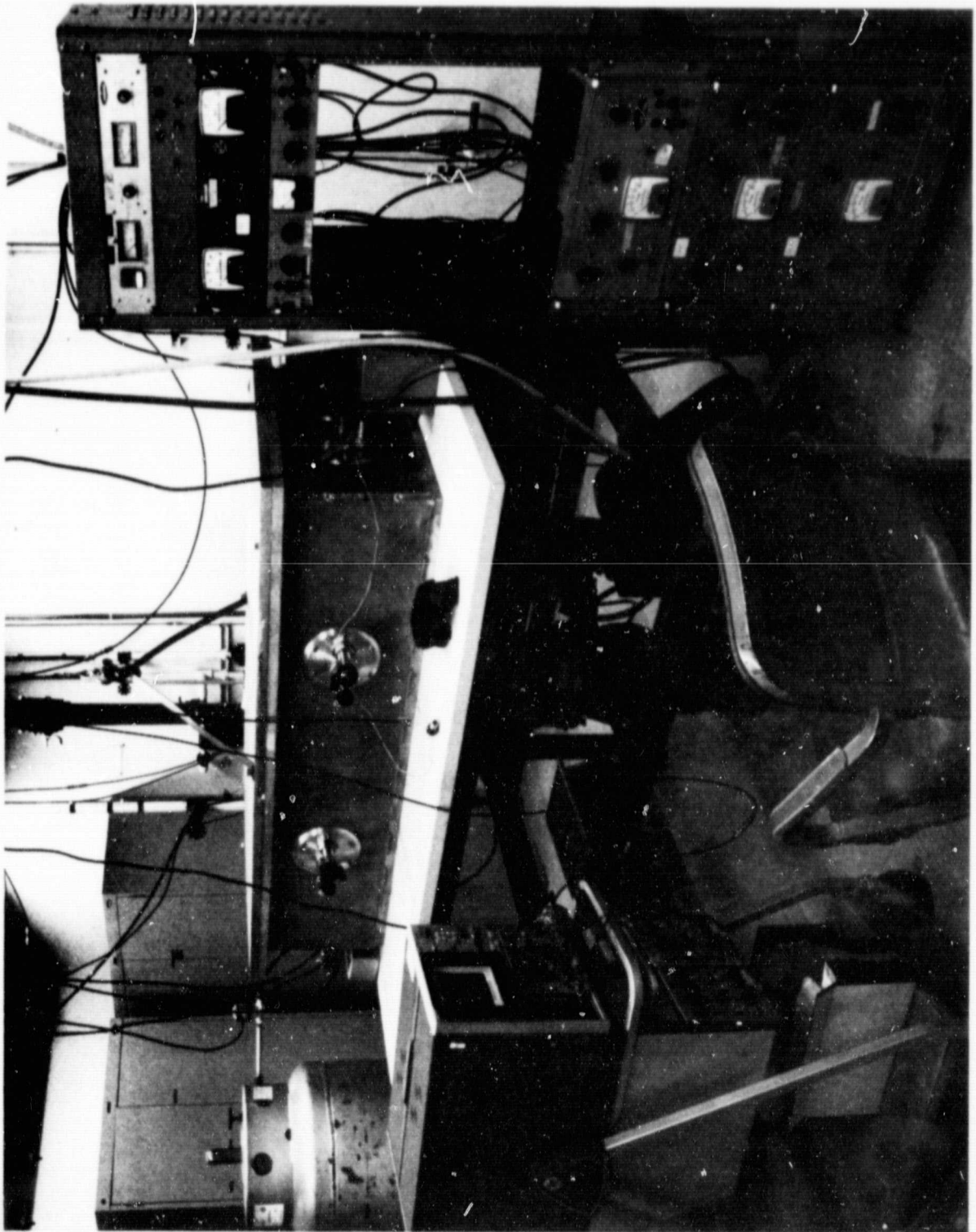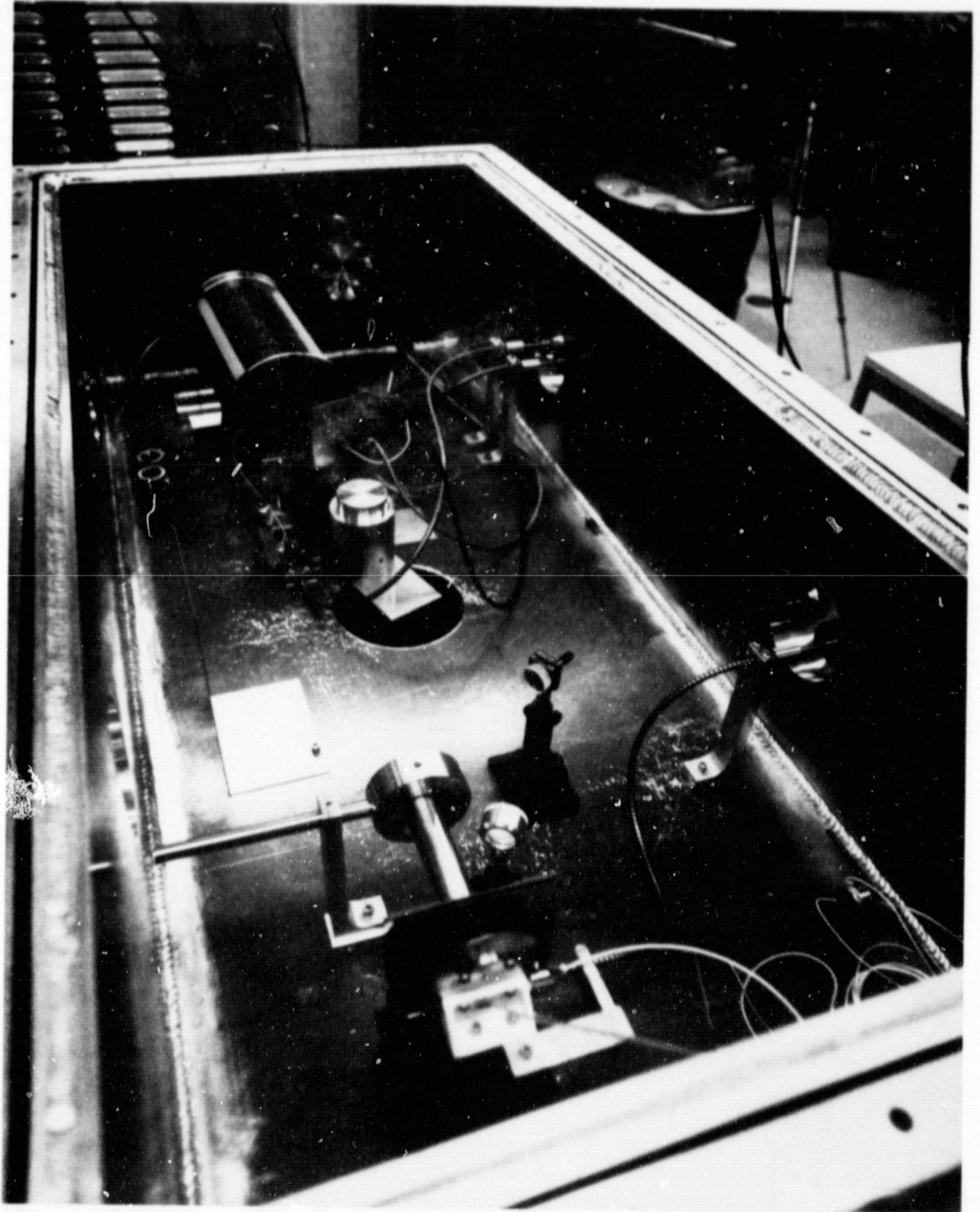
Figure 3.1 Experimental Apparatus

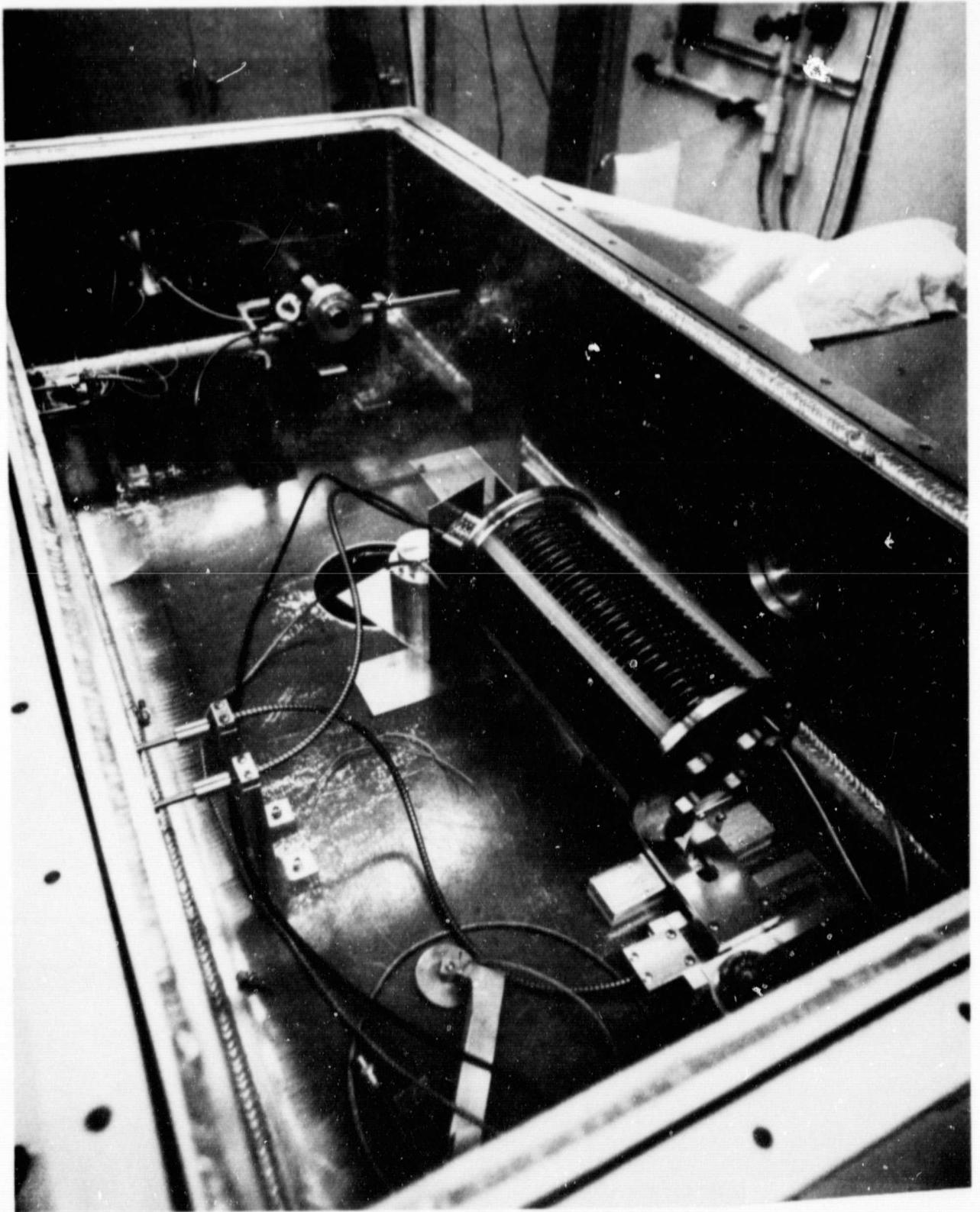Figure 3.2 Internal Apparatus Viewed along Ion Beam Path

26

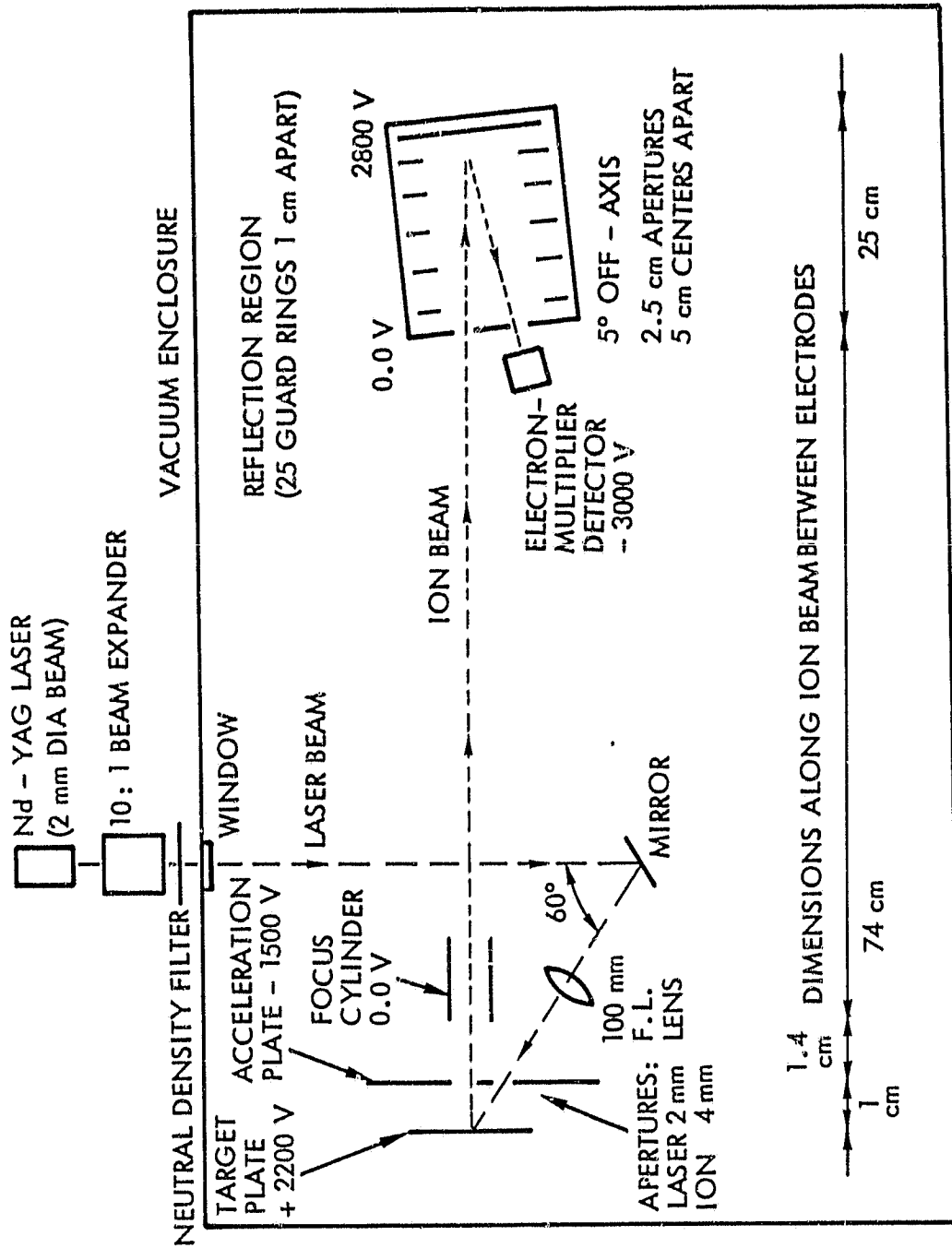Figure 3.3 Internal Apparatus Viewed toward the Laser Target

27

Figure 3.4 Schematic of Experimental Layout

3.1.1 Neodymium-YAG Laser

The tiny Nd-YAG laser is shown in Figure 3.5. Its dimensions are a few centimeters, and with its power supply weights 300 grams. It produces a 7×10^{-3} Joule pulse lasting 10×10^{-9} seconds at a wavelength of 1.06 micrometers. The beam has a diameter of 2 mm, which after expansion to 20 mm with a 10:1 beam expander can be focused with a high quality 100 mm lens to a 15 micrometer diameter spot on the target (sample). In order to reduce the total number of ions produced to a usable value ($\sim 10^6$ ions), neutral density filters are placed in the laser beam path after the expander to cut the energy by a factor of 200 or more. This reduces the total energy on target to 35×10^{-6} Joules, producing a power density of 2×10^9 watts/cm^2.

The laser was manufactured by International Laser Systems, Orlando, Florida, for a hand-held rangefinder, and is very rugged. It is passively (dye-bleach) Q-switched, making it ideal for our purposes. It requires a power input sufficient to charge an 11 microfarad capacitor to 780 V for each laser pulse. With its present power supply, it requires + 5V at 350 ma peak for 6 seconds charging, that is, less than 10 watt-seconds per pulse.

3.1.2 Target Region

The laser target materials (samples for analysis) used in the current contract period consisted of small flat plates of aluminum, stainless steel 304, and coin silver. Aluminum was used predominantly because it yielded simple mass spectra with a single large peak of mass 27$^+$ ions along with smaller impurity peaks at 23 (Na$^+$) and 39 and 41 (K$^+$). The smaller peaks were useful for calibrating the absolute mass scale and comparing plasma bubble temperatures. Aluminum gave consistent and reproducible results which were essential to choosing operating parameters and comparing experimental and theoretical results. Stainless steel 304 was used to demonstrate analysis of a more complex alloy, and was therefore useful in comparing signals from the various atomic species to determine the relative detection efficiencies. The silver target was used to demonstrate the mass resolution between almost equal mass peaks at 107$^+$ and 109$^+$. The target plates were mounted flush at the center of an 8 cm
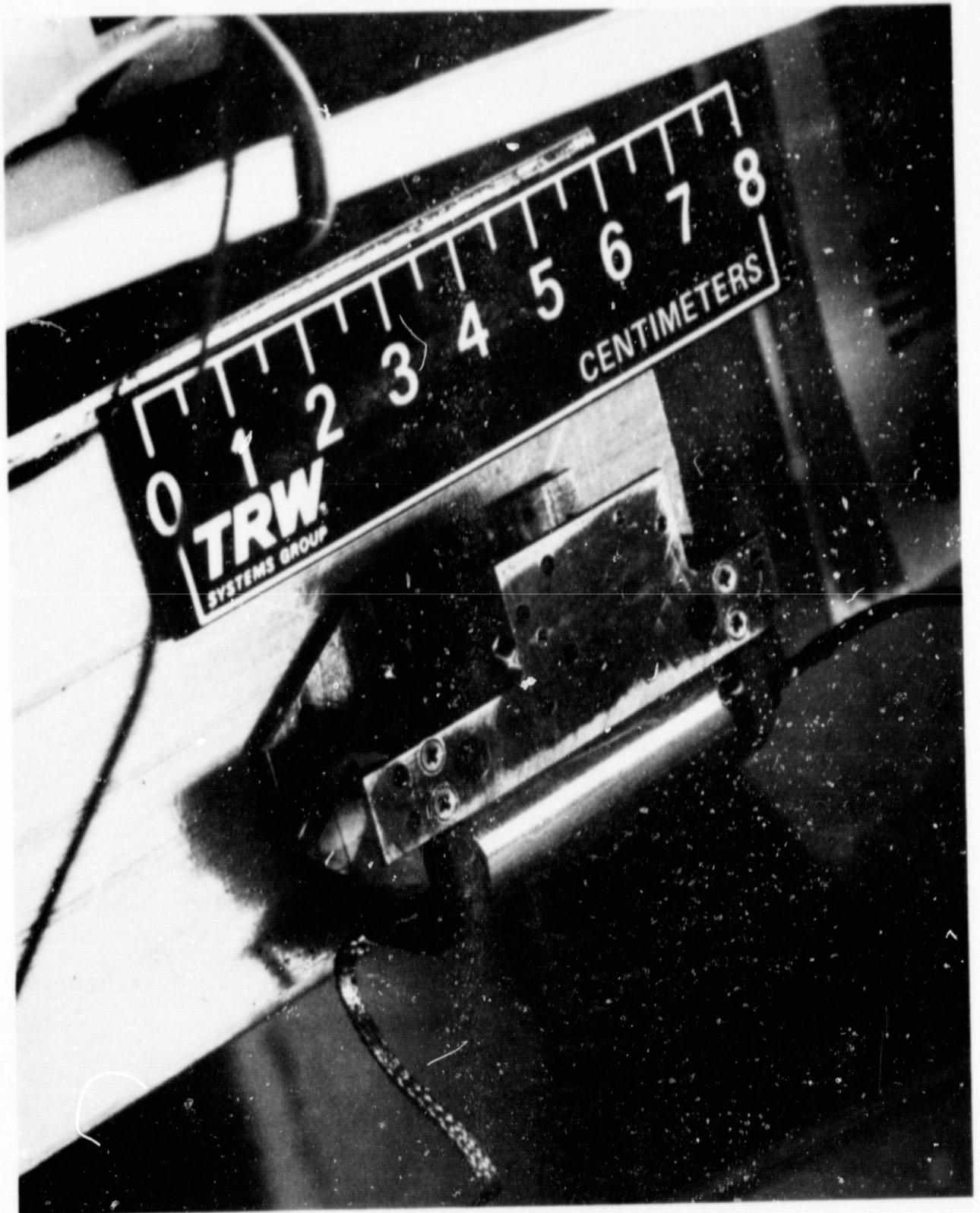
Figure 3.5 Nd-YAG Laser. Beam exists to right parallel to the cm scale

diameter brass target electrode.

A thin flat extraction electrode was placed parallel to the target electrode with a 1 cm spacing, and having a 4 mm diameter hole centered over the laser spot position for passage of the ions after acceleration. A 2mm hole in the plate admitted the laser beam. Beyond the extraction plate was a 2.5 cm diameter x 15 cm long copper cylinder 1.4 cm beyond used for slight ion beam focus. Its axis was along the beam line defined by the laser spot and extraction plate hole. Nominal operating voltages were +2200V, -1500V, and 0V(grounded to vacuum enclosure) for target, extraction, and focus electrodes, respectively. After acceleration, the 2200 eV ion beam passed 74 cm through an electric field-free region to the entrance of the reflection region. The ion beam diameter at 46 cm was measured to be 2 to 3 cm under the operating conditions used.

The vacuum chamber was maintained at 3×10^{-6} mm Hg with a liquid nitrogen-trapped oil diffusion pump

An electronic integrating circuit was connected in series with the target electrode power supply so as to measure the total positive charge (number of singly-charged ions) produced in each plasma bubble. The maximum sensitivity was about 1×10^6 ions, which was around the value usually used.

3.1.3 Reflection Region

The uniform electric field for the reflection region was produced within a structure consisting of 25 concentric insulated stainless steel guard rings spaced 1 cm apart, each of thickness 0.05 cm. The guard rings were connected by 25 one megohm resistors to form a linear voltage divider to supply appropriate potentials to the rings. This configuration produces a highly uniform electric field within the region 10 cm diameter by 25 cm long ($\pm$ 1%). Entrance to the region is through gridded apertures, and each end is terminated by a flat conducting surface, one at ground potential and the other at nominally + 2800 V to produce the correct reflection path length.

The entrance and exit apertures are placed symmetrically about the reflection region axis, are 2.5 cm in diameter, and have centers 5 cm apart.

The reflection region axis can be remotely rotated about the inter-section of the ion beam and center of the entrance aperture. This allows adjustments for optimum ion beam transmission to the detector.

3.1.4 Detector and Electronics

Ions exiting the reflection region were accelerated into a Johnston Laboratories, Inc., Cockeysville, Md., ion-electron multiplier MM1-1SG. Multiplier voltages between -2200V and -3400V were used, corresponding to gains of 2×10^4 and 4×10^7. Final dynodes were capacitor-bypassed. A 1 megohm resistor was connected between the anode and ground to provide a DC path, and a 50 ohm coaxial cable was connected with very short leads across anode and ground. The other end of the cable was connected through BNC hardware directly to a Tektronix Model 7844 oscilloscope with a 50 ohm input 7A24 plug-in with 5 mV/cm sensitivity. No digital data handling was utilized during the current period.

3.2 PREVIOUS EXPERIMENTAL RESULTS

3.2.1 Major Conclusions Reached from Earlier Experiments

During the course of earlier experiments, it became evident that two key requirements on the laser-produced plasma bubble are critical for the success of the program. These two requrements further imply a particular set of laser beam qualities, including sampled-spot size, energy, and time duration.

Requirement A: The first requirement is that the bubble temperature must be high enough for a sufficient time at the bubble atom number den-sity produced so that a high fraction of atoms are ionized, and so that the fraction ionized depends little on species ionization potential. It appears from this current work, and from the work of others,* that this

---

* F. Hillenkamp, E. Unsöld, R. Kaufmann and R. Nitsche, Appl. Phys. 8, 341 (1976);

  R. Wechsung, F. Hillenkamp, R. Kaufmann, R. Nitsche, H. Vogt, 1979 Conference Scanning Electron Microscopy, Los Angeles, April 17-21, 1978;

  J. F. Eloy, Int. J. Mass Spectrom. Ion Phys. 6, 101 (1971);

  N. C. Fenner and N. R. Daly, Rev. Sci. Instr. 37, 1068 (1966).

requirement can be met and that it depends on reaching a laser beam power density of 10^9 to 10^{10} watts/cm^2 for laser pulse durations of tens of nanoseconds (and this short pulse duration is itself a requirement for the time-of-flight mass spectrometer). Unfortunately, a laser was not available to the earlier project which would meet Requirement A and at the same time Requirement B (to be discussed below). That is, although the required power density could be obtained, the sampled area had to be so large that too much plasma was produced for the electric accelerating field to handle. Therefore, in order that Requirement B (below) be met, power densities were limited to the order of 10^7 W/cm^2. As will be discussed in detail in the next section (3.2.2), the appearance of molecular ions and disproportionately high numbers of ions from species with low ionization potentials indicates that the power density reached a barely useful level. Indeed, at somewhat lower power densities, sometimes no ions at all could be detected. On the other hand, by examining the work from the references in the preceding footnote, it became clear that the desired results could be obtained at the 10^9 to 10^{10} W/cm^2 level. A suitable laser was obtained for use during the current contract phase.

Requirement B: The second key requirement is that the total amount of plasma produced be small enough so that an electric field of kilovolts/cm can separate the plasma charge in the expanding bubble in a distance of mm. (It appears from the current work to be described later that this implies a production limit of less than 10^7 ions per laser pulse). A great deal of time was spent in obtaining data where it was later found that the plasma bubble was large and dense enough so that part of it expanded as a neutral fluid clear across the accelerating region, and without acceleration. Under such conditions the results were extremely non-reproducible and confusing. Although it may be noted that Eloy (see preceding footnote) was able to handle above 10^{11} ions per shot, he also allowed the bubble to expand several centimeters before it was accelerated to 8 kV. These parameters are unacceptable for a TOF instrument; Eloy used a magnetic spectrometer with photographic plate detection. (It may also be noted that Eloy's power density was only 10^8 W/cm^2, lower than Requirement A; however, his laser pulse duration was 200 nanoseconds which apparently compensated for the lower power density.)

In order to fulfill Requirements A and B at the same time, it appears necessary to limit the total laser energy to less than 10^{-4} Joules for 10 nanosecond pulse durations. Higher total energy injected at the required temperature produces too many ions. This total energy limit coupled with Requirement A then requires a very small spot size. The projected laser beam parameters which should satisfy Requirements A and B simultaneously are given in Table 3-1.

Table 3-1. Projected Laser Beam Parameters

Spot diameter	10×10^{-4} cm (10 µm)
Pulse Duration	10×10^{-9} sec
Total pulse energy	0.1×10^{-3} Joules
⟶ Power density	10^{10} watts/cm^2

For the earlier measurements and results to be discussed in the next section, the minimum spot size obtainable with the laser and optics used was about 300 µm. If a total laser energy greater than a few tenths mJ was used, Requirement B was obviously violated and meaningless results were obtained. However, with a total laser energy of 0.1 mJ, pulse duration 10×10^{-9} sec, and a spot diameter of 300 µm, the power density was only of order 10^7 W/cm, thereby violating Requirement A. The solution is, of course, to lower the total energy somewhat further and at the same time reduce the spot size to about 10 micrometers. Apparatus with these capabilities was obtained for the current contract phase.

3.2.2 Earlier Experimental Data

Figure 3-6 shows a series of tracings from Polaroid photographs of oscilloscope traces of ion detector current versus time. Table 3-2 lists the parameters used. Note that a constant laser spot size of 1 mm diameter was employed throughout. (Very different from the current spot size). This spot size implies a laser energy for trace (a) of 1.1 Joules, and thus all traces were taken under conditions that grossly violated Requirement B discussed in the preceding section. However, no acceleration was present, so these traces were valid representations of the freely expanding plasma, that is, the initial plasma bubble conditions. Of particular interest in Table 3-2 is the ion energy at the distribution peak of several hundred eV, which is rising fairly slowly with power density at the higher power densities. This appears consistent with the expectation to be able to handle initial energies through energy-time focus to be described in Section 4. Also of particular interest in Table 3-2 is the rapid fall-off in number of ions produced, with power density. Actually, this is due to two effects, first, a linear decrease with total laser energy at the high power densities. This is important in meeting requirement B as discussed in the previous section, and implies the necessity for much lower total laser energy, but with constant power density. Second, a faster fall-off sets in at lower power densities, corresponding to fewer ions produced per Joule of total laser energy and appears to be due to the lower power density. In fact, a threshold behavior occurs at even lower power density, where small random variation in total laser energy caused huge variations in total ion pulse current. However, because of Requirement A (previous section), this low power density regime is of no interest here.

100 mV/div   20 μ sec/div   (a)

100 mV/div   20 μ sec/div   (b)

50 mV/div   20 μ sec/div   (c)

10 mV/div   20 μ sec/div   (d)
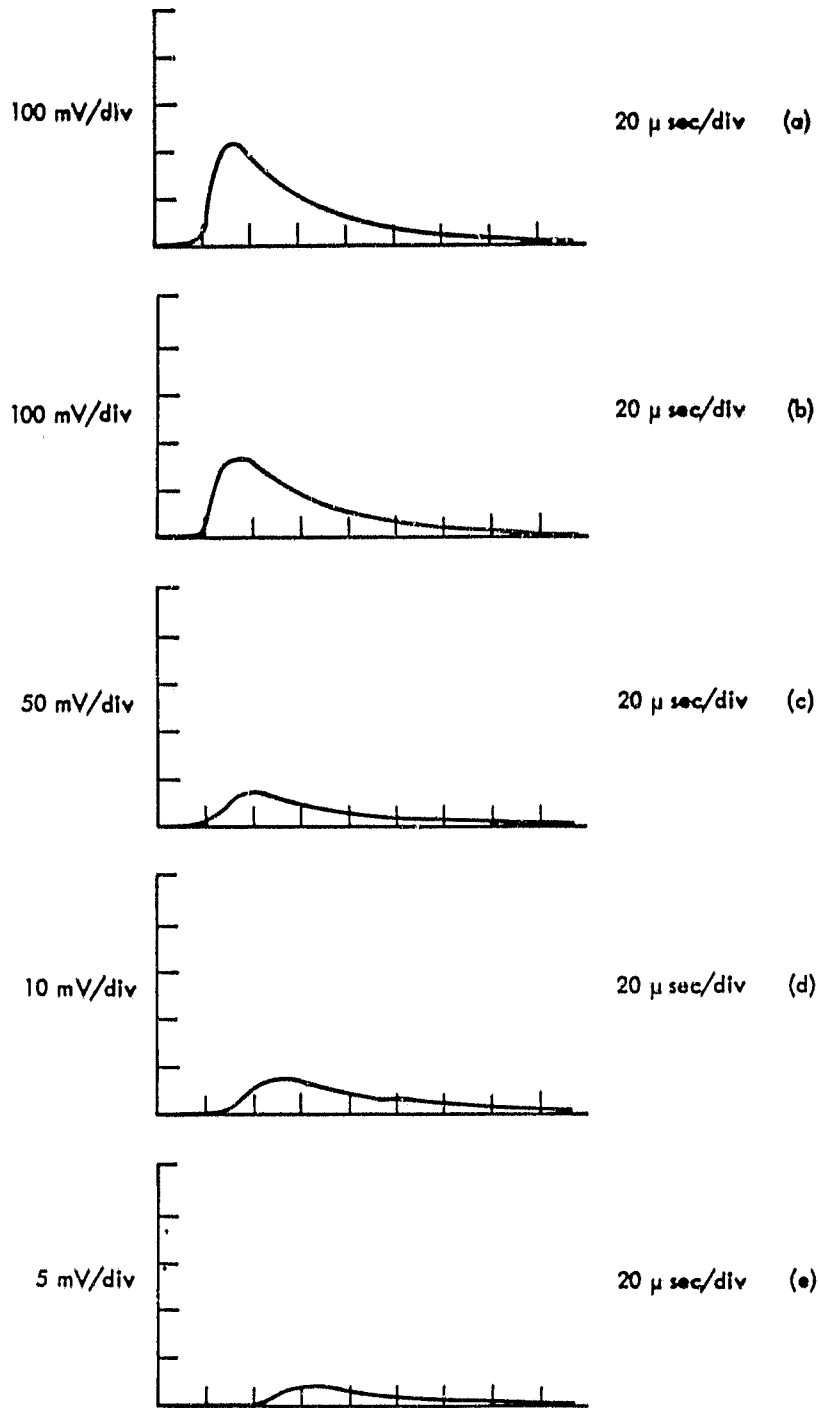
5 mV/div   20 μ sec/div   (e)

Figure 3-6.   Pulse Time Profile vs. Laser Power Density.

Table 3-2. Ion Pulse Parameters as a Function of Laser Power Density

(Material: Nickel; Laser: Ruby; Laser Spot Size: 1 mm dia;
Laser Pulse: 80 nsec; Flight Length: 110 cm; Pulse Time
Profiles: Figure 3-6)

Profile (Fig. 3-6)	Laser Power Density (x 10^8 W/cm^2)	Ion Energy at Peak (eV)	Peak Ion Current (arbitrary units)
(a)	18	360	1.0
(b)	13	320	.7
(c)	4.0	230	.2
(d)	1.8	140	.03
(e)	1.1	85	.01

Figure 3-7 shows oscilloscope traces for samples of aluminum and nickel, with accelerations to 200 V and 400 V respectively, and a flight length of 110 cm, but without energy-time focus. Although Requirement B appears almost met, Requirement A is very far from being met. This can be seen from the predominance of Na^+ and K^+, which are from trace elements with very low ionization potentials. The power density here was less than 10^8 W/cm^2, but the poor quality spot was not well defined. The ion peaks occur at times corresponding to essentially the acceleration energy. This implies either very little initial kinetic energy, or less than full acceleration across the accelerating region.

Figure 3-8 shows ion arrival time traces from a lead sample. Trace (a) is without acceleration and shows an initial energy at the peak (large peak) for Pb^+ of 200 eV. Much smaller peaks corresponding to Na^+ and K^+ still appear. Trace (b) is with 1500 V acceleration but without energy-time focus. The large peak (Pb^+) occurs at a time corresponding to an energy of 1200 eV, thus implying that the plasma expanded well into the accelerating region and did not gain the full acceleration. That is, both Requirements A and B were violated. A very interesting phenomenon appears in trace (b), namely that a series of ions Pb_n^+, with n going from 1 to at least 6 appears to be produced under the laser bombardment conditions obtaining here. The power density was between 10^7 and 10^8 W/cm^2, but the laser spot was TEM_{00} as contrasted to Figure 3-7 in which a multimode spot was used. Hence, a direct comparison of power density is difficult.

Figure 3-9 shows traces from a sample of 50-50 tin-aluminum alloy. The flight length was 63 cm, and no energy-time focus was used. Again Requirements A and B are violated. Thus, at the insufficient power density obtaining for trace (a), a series of molecular ions is observed. The power density for trace (b) was somewhat higher, but this caused a greater violation of Requirement B, while improving on Requirement A. In this case roughly equal amounts of the major species were observed, with much fewer molecular ions.

The results of the current work will be presented in Section 5, and will show great improvement toward meeting Requirements A and B.
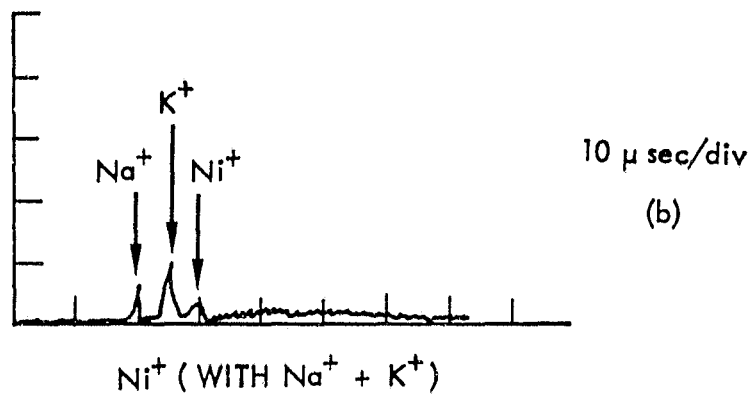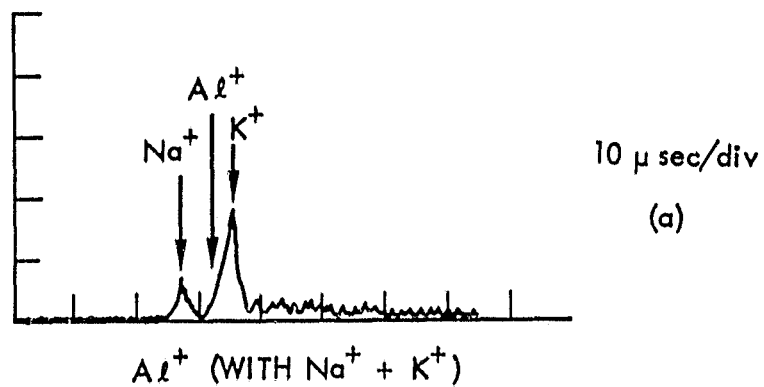
Figure 3-7. Aluminum and Nickel Targets at Very Low Power Density.

Pb^+ (WITH Na^+ AND K^+)

NO ACCELERATION

20 μ sec/div

(a)

Pb^+ (WITH Pb_n^+)
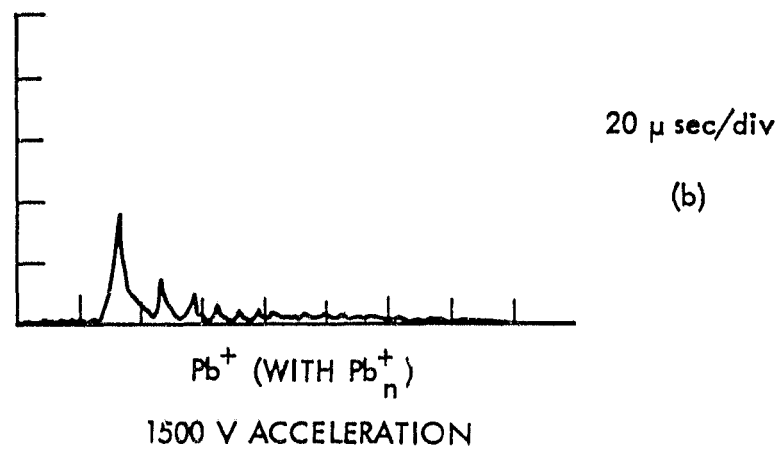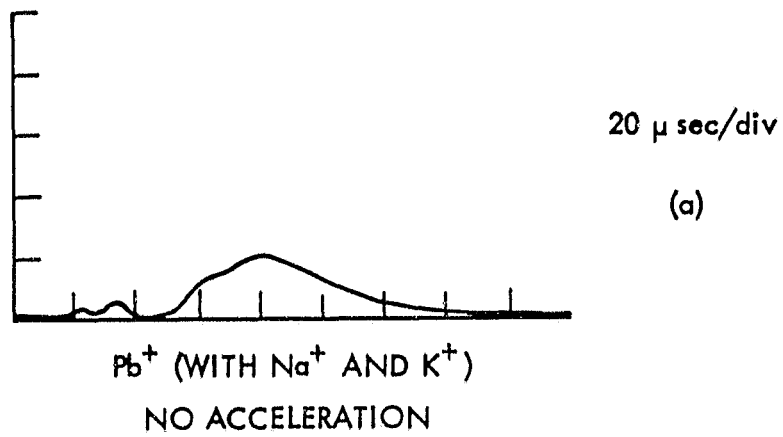
1500 V ACCELERATION

20 μ sec/div
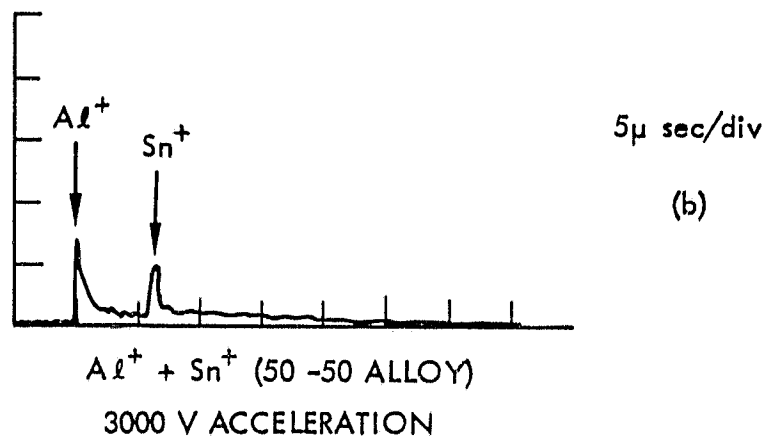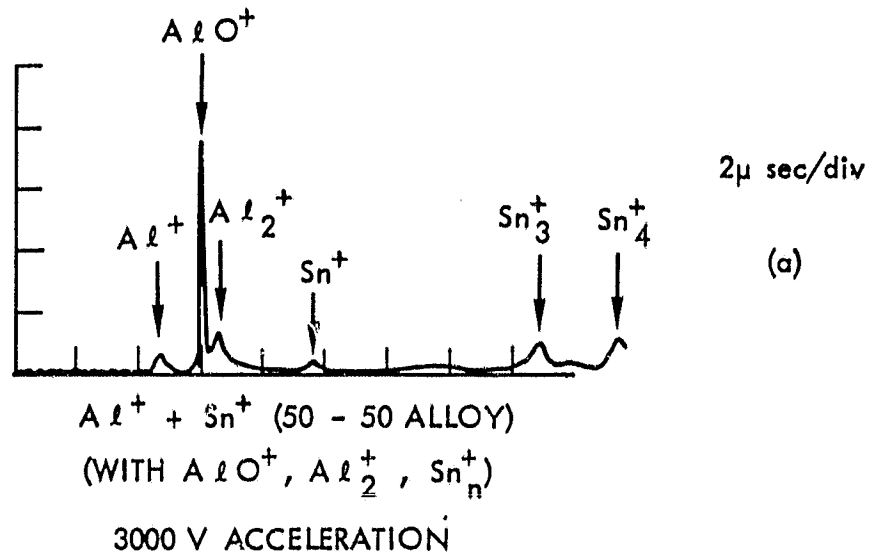
(b)

Figure 3-8. Lead Target at Low Power Density.

Figure 3-9. Tin and Aluminum Alloy Target at Low Power Density.

4. ENERGY-TIME FOCUS FOR TIME OF FLIGHT MASS SPECTROMETERS

4.1 INTRODUCTION

A time-of-flight (TOF) mass spectrometer operates on the principle that particles with the same kinetic energy but with differing masses have different speeds and, therefore, traverse the same path between two points with different "flight times." By measuring the particle arrival times it is possible to associate the arrival times with the particle mass and thereby determine the "mass spectrum" of particles passing through the TOF instrument. In order that the arrival times for all particles of a given mass be identical, it is necessary that they all start their "flight" at the same time with the same kinetic energy. In any practical instrument there always exists a spread in both starting time and energy, and the amount of spread determines the "mass resolution." That is, if the spread in starting times for particles of two masses is greater than the difference in their flight times, their arrival time peaks will overlap and they will not be resolved. Initial energy spread has a similar effect by also broadening the arrival-time peaks for individual masses.

The energy-time focus device described here reduces drastically the effect of initial energy spread by adding additional flight-time to all particles (ions), with more being added to the initially faster ions which would otherwise arrive "too early." That is, the normal flight-time plus the added time in the device sums to a total time which is largely independent of the initial energy. Therefore, all ions of a given mass, but with a spread in initial energy, arrive at almost the same time at the detector, and at a time different from other masses. This constitutes essentially an "energy-time focus."

The active element of the device consists of a uniform electric field placed at the end of the normal flight tube of a TOF mass spectrometer. The field strength and direction are adjusted so that the ions are stopped and reflected almost back on their original path in a distance one-fourth the length of the normal flight path. (This assumes a negligible time spent in the first acceleration region, and that the energy due to the first electric acceleration is much greater than the initial

energy spread. The value "one-fourth" may be adjusted slightly to compensate for partial failure of these assumptions.)

Figure 4-1 shows a schematic drawing. A usual TOF mass spectrometer has the detector entrance at the same location, but pointed toward the ion source. The "reflection region" constitutes the device to be described here. It could be appended to any TOF ion spectrometer in which initial energy spread is troublesome, in order to increase mass resolution. The uniform electric field is produced within a series of "guard rings" held at potentials appropriate to produce the necessary uniform electric field. The reflection region is terminated by screens or plates at the ends.
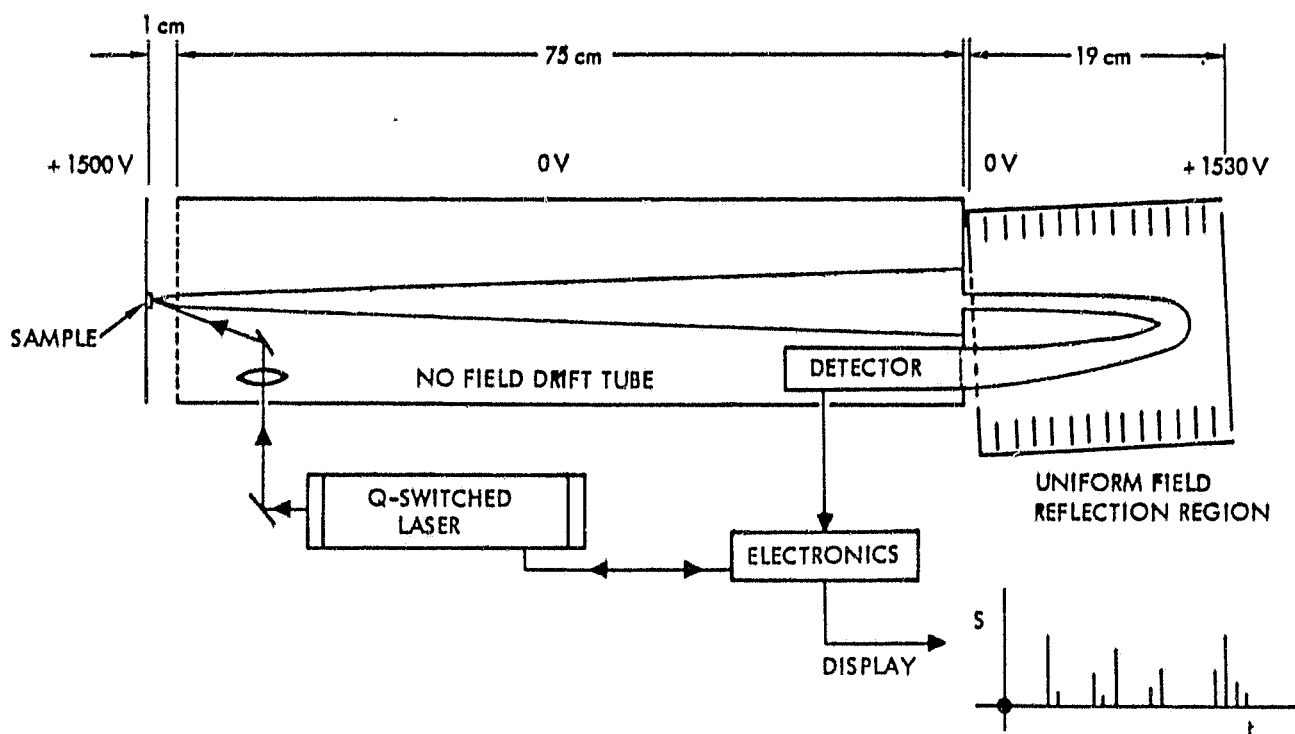

Figure 4-1. Schematic Diagram of TOF Mass Spectrometer with Laser Blow-Off Ion Source and Energy-Time Focus.

43

4.2 THEORY OF ENERGY-TIME FOCUS

In a usual time-of-flight (TOF) mass spectrometer, ions of a given mass will arrive at the detector at precisely the same time only if they travel the same free flight distance after starting at precisely the same time with precisely the same initial kinetic energy. In any practical TOF instrument neither the starting times nor the starting kinetic energies are precisely equal for all ions of even the same mass. Thus, for a free-flight path of length L meters for ions of mass in kilograms with charge q Coulombs accelerated across a potential difference V volts and having initial kinetic energy E_0 Joules, the free-flight time t seconds is given by

$$t = L \cdot \left[2(qV + E_0)/m \right]^{-1/2} \quad . \tag{4.1}$$

Now if all the ions have zero initial energy, the difference in arrival times Δt_m for two masses m and m + Δm is approximately given by

$$\Delta t_m \simeq \frac{dt}{dm} \cdot \Delta m = \frac{d}{dm} \left(\frac{L}{\sqrt{2qV}} m^{1/2} \right) \cdot \Delta m = \left(\frac{Lm^{-1/2}}{2\sqrt{2qV}} \right) \cdot \Delta m \quad . \tag{4.2}$$

This Δt represents the time between the signal "spikes" for masses m and m + Δm. Clearly if the ions of mass m (and/or mass m + Δm) have starting time spreads greater than or about equal to Δt_m, or if the electronic circuitry cannot resolve signal peaks occurring within Δt_m, then masses m and m + Δm will not be resolved by a TOF mass spectrometer with parameter values determining Δt_m through Eq. 4.2. For example, in order to resolve a particular mass m from mass m + Δm, it might be necessary to increase L or reduce V. These considerations are extremely important to the overall conclusion of this report, but it will be assumed for the present discussion that Δt_m for masses m and m + Δm of interest is large compared to starting time spread and electronic detection time resolution. Under this assumption, resolution will be limited by the spreads in initial ion kinetic energy E_0, as seen from Eq. 4.1. The arrival time difference Δt_{E_0} for two ions of mass m, but having initial energy $E_0 = E_0$ and $E_0 = 0$ is given by

$$\Delta t_{E_0} = L \cdot \sqrt{\frac{m}{2}} \cdot \left\{ (qV)^{-1/2} - (qV + E_0)^{-1/2} \right\}$$

$$= \frac{Lm^{1/2}}{\sqrt{2qV}} \cdot \left\{ \frac{E_0}{2qV} + \cdots \right\} \quad . \tag{4.3}$$

When the spread in E_0 becomes sufficiently large, that is, when Δt_{E_0} is larger than or about equal to Δt_m for two masses m and Δm of interest, then m and $m + \Delta m$ cannot be resolved. It may be noted that increasing L does not help in this case since both Δt_m and Δt_{E_0} increase linearly with L. Increasing the acceleration voltage V does reduce the effect of E_0, but at the cost of decreasing Δt_m for a given m and $m + \Delta m$ which is eventually limited by starting time spread and electronic detection time resolution as discussed above in this section.

By equating Δt_m and Δt_{E_0} from Eqs. 4.2 and 4.3 and taking $\Delta m = 1$, the following approximate expression is found.

$$m \cong qV/E_0 \quad . \tag{4.4}$$

This implies that the mass number m which can barely be resolved from the adjacent mass number because of mass m having a spread in initial kinetic energy E_0 is given by the acceleration energy divided by the initial energy spread E_0. For the actual TOF spectrometer configuration being considered here, E_0 may easily be as high as 50 eV, while length L and starting time considerations limit qV to 1500 eV. Thus, masses higher than mass 30 would not be resolved. Clearly this is unacceptable, and in order to solve this problem, the following energy-time focus technique was discovered.

The desired result is that two ions of mass m but having differing initial energy $E_0 = 0$ and $E_0 = E_0$ arrive at the detector at the same time, that is, that the flight time not depend on E_0. It is seen from Eq. 4.1 that this is not the case for a simple free-flight TOF spectrometer. However, by adding a "reflection region" to the total flight path in which the ions slow to a stop and are reflected back to the detector, it is possible to produce a total travel time which is independent of initial energy to second order in E_0/qV, and for which this "focus"

45

condition does not depend on m. Consider the time trajectory of an ion entering a uniform electric field, $\vec{\epsilon}$, whose direction is opposite to the velocity v_0 of the ion when it enters the uniform field region. Let x, v, and a represent the distance traveled in the direction against the field, the speed along x, and the acceleration along x, respectively. $-\vec{\epsilon}$ is also along x, so the problem is one dimensional, and

$$a = \frac{-q\epsilon}{m} \tag{4.5a}$$

$$v = \frac{-q\epsilon}{m} t + v_0 \tag{4.5b}$$

$$x = \frac{-q\epsilon}{2m} t^2 + v_0 t \quad . \tag{4.5c}$$

The time to reflect back to the starting (entry) point, t_r, is twice the time to stop, t_s, which is given from Eq. 4.5b as

$$t_r = 2 \cdot t_s = 2 \cdot \frac{v_0 m}{q\epsilon} = \frac{2m}{q\epsilon}\left[\frac{2}{m}(qV + E_0)\right]^{1/2} \quad . \tag{4.6}$$

The total flight time t_T for an ion is then the free flight time given by Eq. 4.1 plus the reflection time t_r given by Eq. 4.6.

$$t_T = L \cdot \sqrt{\frac{m}{2}} \cdot (qV + E_0)^{-1/2} + \frac{2m}{q\epsilon}\sqrt{\frac{2}{m}} (qV + E_0)^{1/2} \quad . \tag{4.7}$$

Now if one makes the stopping field ϵ

$$\epsilon = 4 \cdot V/L \quad , \tag{4.8}$$

one obtains the result

$$t_T = L \cdot \sqrt{\frac{m}{2}} \cdot \frac{1}{\sqrt{qV}} \cdot \left\{ (1 + E_0/qV)^{-1/2} + (1 + E_0/qV)^{1/2} \right\} \tag{4.9}$$

and expanding,

$$t_T = L \cdot \sqrt{\frac{m}{2}} \cdot \frac{1}{\sqrt{qV}} \cdot \left\{ 1 - \frac{E_0}{2qV} + \frac{3E_0^2}{8q^2V^2} - \dots + 1 + \frac{E_0}{2qV} - \frac{E_0^2}{8q^2V^2} + \dots \right\}$$

$$= 2 \cdot L \cdot \sqrt{\frac{m}{2}} \cdot \frac{1}{\sqrt{qV}} \cdot \left\{ 1 + \frac{1}{8}\left(\frac{E_0}{qV}\right)^2 - \dots \right\} \quad . \tag{4.10}$$

46

Upon inspection of Eq. 4.10 it may be seen that the total flight time t_T is, to first order, just twice the normal TOF flight time without a reflection region for an ion with $E_0 = 0$, as given in Eq. 4.1; furthermore, the first order terms in E_0/qV cancel out along with a fraction of the second order terms. For this case the $\Delta t_{T,m}$ time difference between arrival of masses m and m + Δm is twice Δt_m from Eq. 4.2,

$$\Delta t_{T,m} \cong \left(\frac{Lm^{-1/2}}{\sqrt{2qV}} \right) \cdot \Delta m \qquad (4.11)$$

and in analogy to Eq. 4.3 for two particles of mass m but with $E_0 = 0$ and $E_0 = E_0$, the $\Delta t_{T,E_0}$ is given by

$$\Delta t_{T,E_0} \cong - 2 \cdot L \cdot \sqrt{\frac{m}{2qV}} \cdot \frac{1}{8} \left(\frac{E_0}{qV} \right)^2 \qquad . \qquad (4.12)$$

Again in analogy to obtaining Eq. 4.4, if $\Delta t_{T,m}$ and $\Delta t_{T, E_0}$ in Eqs. 4.11 and 4.12 are set equal and Δm = 1, one obtains

$$m \cong 4 \left(\frac{qV}{E_0} \right)^2 \qquad . \qquad (4.13)$$

This implies that the mass number m which can barely be resolved from the adjacent mass number because of m having an initial energy spread E_0 is not reached until mass 3600 for an acceleration to 1500 eV with E_0 = 50 eV. This is contrasted to a limit of mass 30 for the same TOF conditions without the energy-time focus reflection region, as discussed with Eq. 4.4. It is not likely that a resolution of 3600 will be reached here because of starting time spread and three-dimensional effects in the reflecting region, since the ions must be reflected at a slight angle in order to reach a detector outside the original ion path before reflection.

Equation 4.8 states the condition on the reflecting ε field magnitude which must be satisfied to obtain energy-time focus. Consider first an ion with E_0 = 0. It must reach a potential equal to V at the time it stops and reverses, and the distance X it traverses to that point must satisfy

$$\varepsilon \cdot X = V \qquad , \qquad (4.14)$$

47

but Eq. 4.8 requires that $c = 4 \cdot V/L$. Hence

$$X = L/4 \quad , \tag{4.15}$$

is the necessary condition on X. That is, the field must be uniform and such that an ion with $E_0 = 0$ stops and reflects at a distance into the reflection region of $L/4$, where L is the normal TOF flight path without energy-time focus.

The reflection region must be long enough to accommodate ions with initial energy $E_0 > 0$. However, it is possible to utilize an end plate on the reflection region to remove particularly high energy ions from the "tail" of the initial energy distribution, thereby providing a low pass energy filter to limit the energy spread E_0.

The theoretical value "4" required by Eq. 4.8 is correct for the ideal case where all ions start at the same time into the free-flight region, and are reflected exactly back along their original paths in the reflection region. It is likely that for a practical instrument, where ions are first accelerated over a finite region before entering the free-flight region and are reflected at a slight angle to the detector and where some space charge effects may become significant, the best number may not be "4". Indeed, the computer simulation to be described next indicated that "3.8" was a better value for the specific parameters used. This is easily varied in practice by varying the potential across the length of the reflection region to "tune" the focus.

4.3 COMPUTER SIMULATION OF TOF SPECTROMETER WITH ENERGY-TIME FOCUS

As a major part of the program to show feasibility for a laser blow-off time-of-flight mass spectrometer for cometary particulate analysis, a one-dimensional Monte Carlo computer simulation was developed. The computer simulation program evolved over the course of the project as new approaches and techniques were added or discarded. It became evident very early that the spread in ion initial kinetic energy of 10's to 100's of eV presented a severe problem if mass resolution of 100 was to be obtained while maintaining an overall length less than one meter.

This evolution eventually led to the energy-time focus technique discussed above in Section 4.2, which appears to have solved the problem

of initial ion energy. Although the earlier ideas and attempts were unsuccessful, they will be discussed briefly in the interests of complete documentation.

All versions of the computer simulation have included a Monte Carlo random choice for each ion of starting time after zero, initial position in the first acceleration region, and initial kinetic energy. Starting time distributions were represented by the same function as the charge and discharge of a simple RC electrical network, with an exponential rise followed by an exponential decay back to zero. The RC time constant and the number of time constants for "on" could be chosen. Thus, an RC of one nanosecond, "on" for 30 time constants produces an almost uniform distribution lasting 30 nanoseconds; a peaked distribution results from "on" of a few time constants. This distribution was originally picked to simulate ions produced by a pulsed electron beam, for which the distribution is a good representation. It is adequate to show "worst case" simulation for the laser produced plasma under the assumption that ions are only produced during the laser pulse. Implicit in this assumption is negligible "extraction time" for ions from the plasma bubble by the electric field; actually the bubble must expand to some degree before the ions "su.⁻t". This part of the simulation becomes more accurate as the total number of ions produced decreases to the point where plasma bubble effects are negligible.

The distribution of initial ion positions is represented by a normalized polynomial ($1 + ax + bx^2 + cx^3$) for x in centimeters. If the polynomial becomes negative, the distribution is taken as zero from that point on. For example, if b is -400 then the distribution falls from maximum at x = 0 quadratically to zero at x = 0.05 cm. Again, this distribution was originally used to represent the distribution of electrons in a pulsed ionizing electron beam, which determined the ion initial position distribution. In the case of the laser blow-off-produced plasma bubble, this distribution can be used to determine an estimate of the "worst case" effect for a given initial position distribution in the accelerating field. However, since the plasma is conducting to some point in its expansion, the actual spread in final ion energy will be less than in the absence of plasma. This distribution leads to a "worst case" so

49

long as all ions are extracted from the plasma within the region represented by the chosen distribution function parameters. This part of the simulation also increases in accuracy as the total number of ions produced decreases to where plasma bubble effects are unimportant.

The distribution function for initial ion energies (velocities) was taken as a one-dimensional Maxwellian distribution given by

$$dN_x = N \left(\frac{m}{2\pi kT}\right)^{1/2} \exp\left(- mv_x^2/2kT\right) dv_x \quad , \quad (4.16)$$

where N is the total number of ions, m is ion mass, v_x the speed, and kT the Boltzmann energy (temperature). This distribution function is expected to be a good representation of the initial energy of the ions from a freely expanding laser blow-off-produced plasma bubble. Actually, it has been noted earlier[*] that the plasma particle velocities are best represented by a lower thermal temperature coupled to a "blow-off velocity" of the center-of-mass of the bubble. However, the velocity distribution along the normal to the source plane producing the bubble is well represented by assuming a higher temperature (kT) and ignoring the "blow-off velocity." The computer simulation is able to handle a separate "blow-off velocity" parameter, but the facility was not used. In the cases where the plasma bubble does not expand freely, but expands within a strong electric field, the degree of validity is uncertain. However, comparison with results of reported measurements[†] indicates that use of kT = 200 eV produces an initial energy distribution for simulation as broad as or broader than those measured under similar electric field conditions.

With the starting time, position, and initial energy of each ion chosen by random numbers (Monte Carlo), simulations of time-of-flight (TOF) mass spectrometers were made for a number of TOF configurations.

---

[*]N. G. Utterback, S. P. Tang, and J. F. Friichtenicht, Phys. Fluids 19, 900 (1976).

[†]J. F. Eloy, Int. J. Mass Spectrom. Ion. Phys. 6, 101 (1971); E. Hillenkamp, E. Unsold, R. Kaufmann and R. Nitsche, Applied Phys. 8, 341 (1975); N. C. Fenner and N. R. Daly, Rev. Sci. Instr. 37, 1068 (1966).

The simplest consisted of an acceleration region in a uniform electric field followed by a field-free flight region. Figure 4.2 shows the simulated mass (time) spectrum obtained for this configuration for the parameters and Monte Carlo distributions given in Table 4-1, for the example spectrum of masses given in Table 4-2. It is immediately clear from Figure 4-2 that this simple TOF instrument configuration with a laser blow-off ion source is unacceptable if a mass resolution of 100 is to be obtained. Even if the initial energy distribution is determined by kT = 20 eV rather than 200 eV, the same result obtains. For this reason a number of attempts were made via simulations of other techniques and configurations to solve this problem of high initial kinetic energy.

The first attempt involved a time delay after the laser pulse in turning on the accelerating field. This allowed the ions to distribute themselves spatially within the accelerating region according to their initial energy before the accelerating field was established; thus a "faster" ion would have moved further across the acceleration region before the field was applied and would therefore receive less energy from the accelerating field. The initially "slower" ion would then catch up to the initially "faster" ion just at the detector, producing a focus in time for ions of differing initial energy. This scheme does produce a reasonable time focus for a small mass number range for a given delay setting, but the delay setting must be changed for each mass number region to be studied. Furthermore, the focus is not sufficiently independent of initial ion energy to produce fully acceptable results.

A second attempt again involved a pulsed accelerating field, but rather than being turned on and left on after a delay time, the field was turned on and then off before ions reached the end of the accelerating region. This acceleration produced an equal "impulse" for all ions, resulting in mass separation in arrival times varying directly as m rather than $\sqrt{m}$ as with the other techniques. However, the initial energy spread was still sufficient to cause arrival time overlap and unacceptably low mass resolution. Also prohibitively high accelerating potentials and slew rates would be necessary.

A third technique was attempted which involved an energy selector which allowed only a narrow energy spread of ions to pass to the detector,
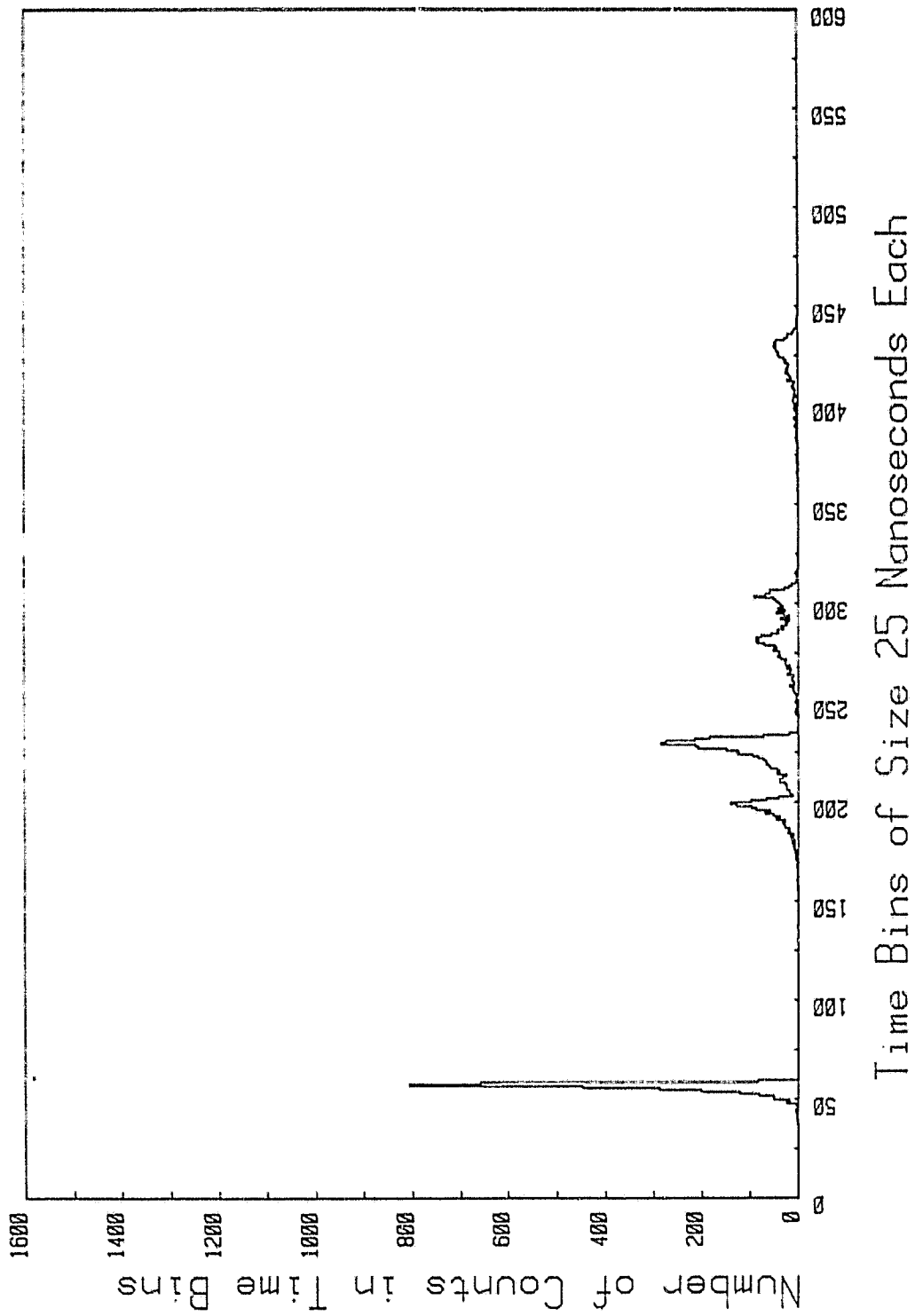
Figure 4-2. Mass Spectrum Without Energy-Time Focus.

Table 4-1. TOF Simulation Parameters and Initial Distributions
            (Figure 4-2)

Length of Acceleration Region	1 cm
Length of Field-free Flight Region	75 cm
Acceleration Energy	1500 eV
TOF Arrival Time Bin Size	25 ns
Number of Particles Injected	10,000 ions
Starting Time Distribution:	
Uniform over first	30 ns
Starting Position in Accelerating Region:	
Quadratic fall-off from maximum to zero in first	0.5 mm
Starting Kinetic Energy Distribution:	
Maxwellian with kT equal to	200 eV

––––– ––––– ––––– –––––

and, in addition, for the case with Energy-Time Focus
(Figures 4-3 and 4-4)

Length of Reflection Region	∿ 20 cm
Reflection Parameter: (simple theoretical value 4)	3.8
Upper Energy Limit: (defined by physical end of reflection region)	1530 eV

Table 4-2. Number Distributions of Masses
for Computer Simulations

SPECIES	MASS	ATOM FRACTION (%)
H	1	28.7
C	12	11.4
C	13	0.1
O	16	28.6
O	18	0.1
Mg	24	9.0
Mg	25	1.2
Mg	26	1.3
Si	28	8.8
Si	29	0.4
Si	30	0.3
Fe	54	0.6
Fe	56	8.9
Fe	57	0.2
Ni	58	0.3
Ni	60	0.1

thus throwing out ions with widely divergent energy and, therefore, having potential arrival time overlap. This technique required an energy selector with unacceptably high energy resolution and low transmission.[†]

Finally, the Energy-Time Focus technique utilizing a reflection region, and described in detail in Sections 4.1 and 4.2, was discovered. It appears to be the solution to the problem of the high initial energy spread. Figures 4-3 and 4-4 show the results with Energy-Time Focus using the same parameters for the TOF simulation as Figure 4-2 (Tables 4-1 and 4-2), but with the added reflection region.

A direct comparison of Figure 4-2 with Figures 4-3 and 4-4 shows the great improvement in mass resolution resulting from Energy-Time Focus with a reflection region.

Section 5 will show experimental results compared to computer simulations of the experimental configurations. It will be seen that the energy-time focus performs experimentally very closely to the theoretical expectations.

[†]It was later discovered that this technique has been previously used, and was limited to a mass resolution of 30. See N. C. Fenner and N. R. Daly, Rev. Sci. Inst. 37, 1068 (1966).
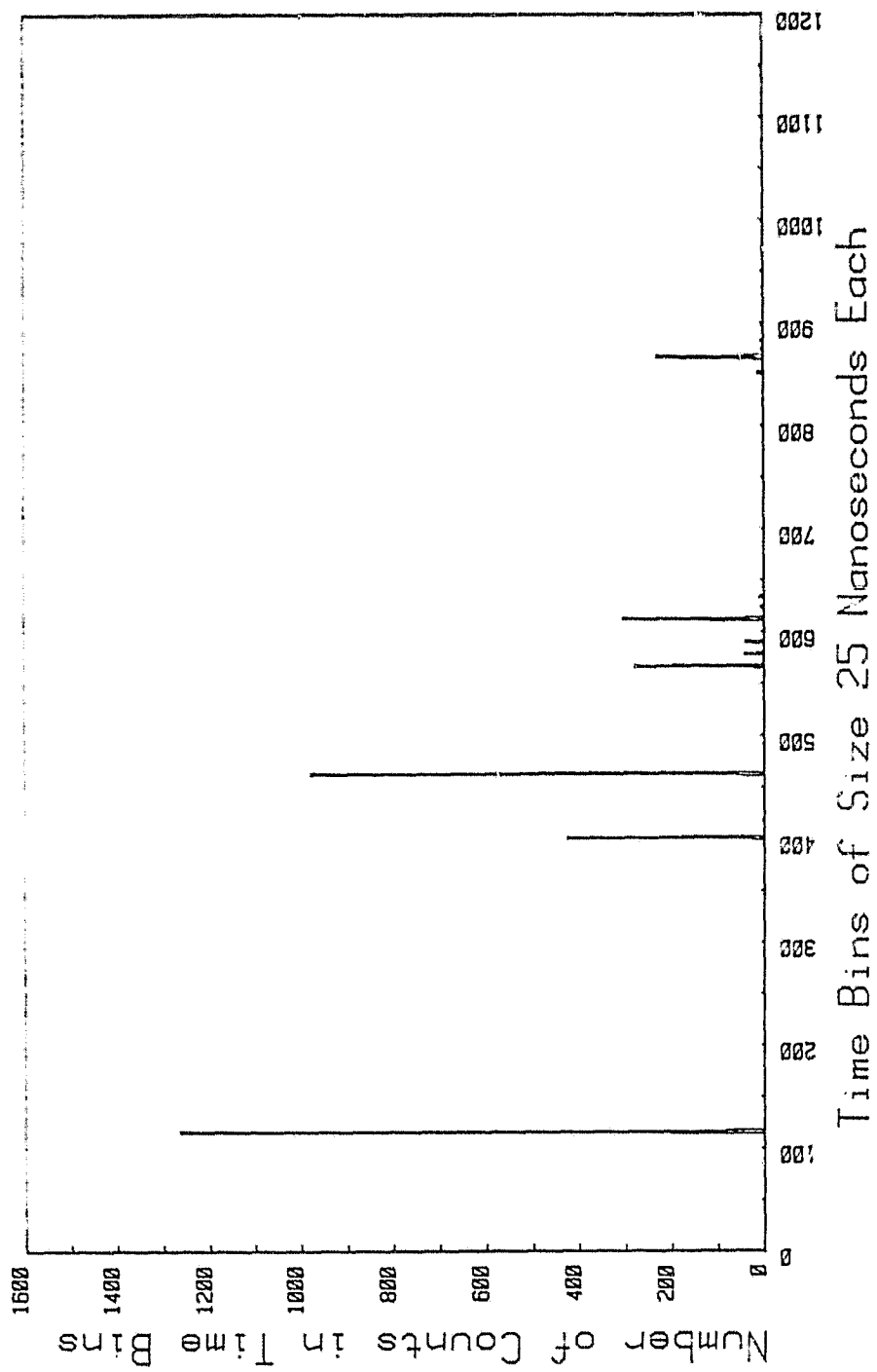
Figure 4-3.   Mass Spectrum with Energy-Time Focus (Low Sensitivity).
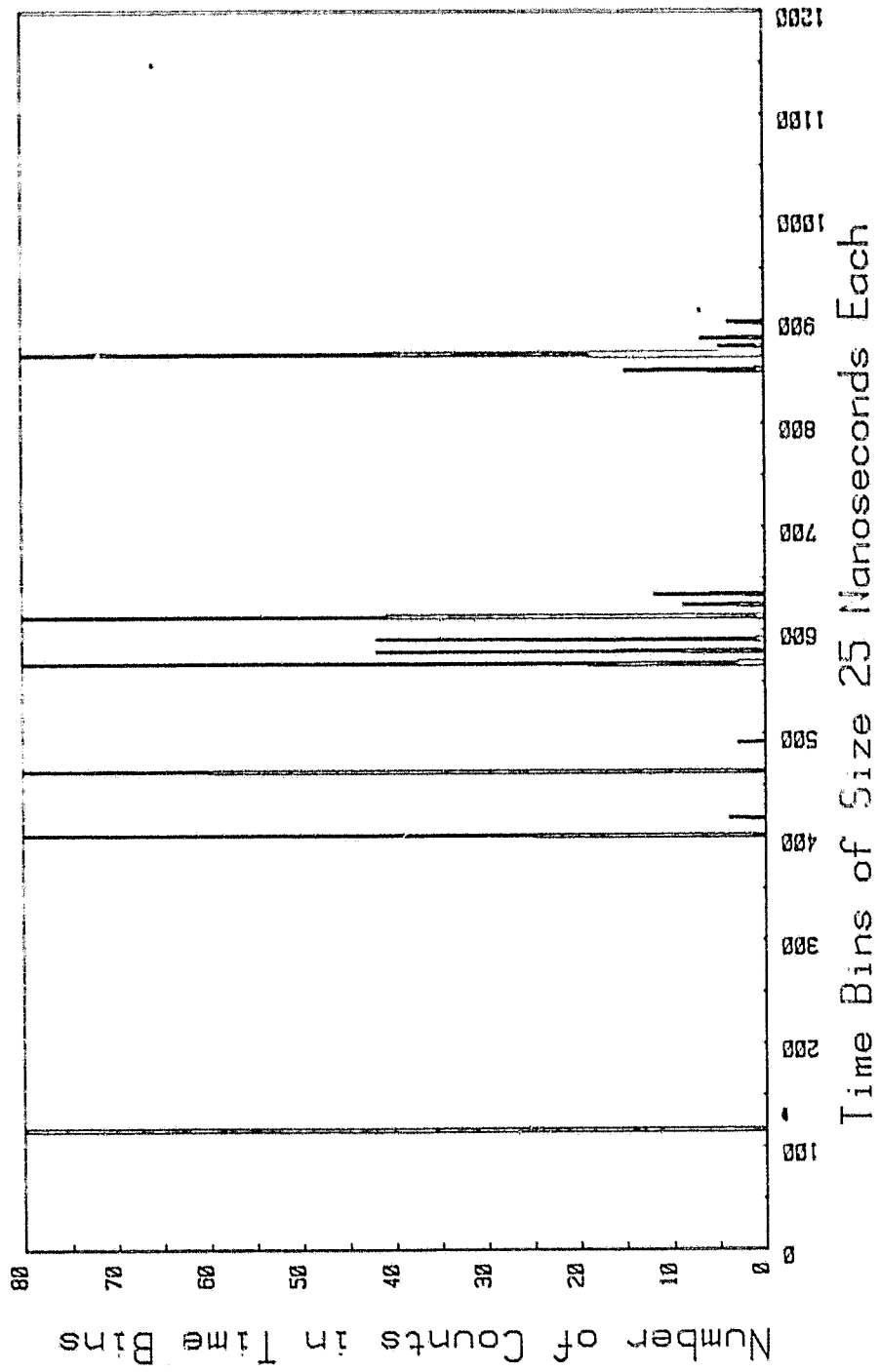
Figure 4-4. Mass Spectrum with Energy-Time Focus (High Sensitivity).

5.0 PRESENT EXPERIMENTAL RESULTS

5.1 PRESENT RESULTS WITHOUT ENERGY-TIME FOCUS

Figures 5-1 and 5-2 (c) show spectra obtained directly as pictures of oscilloscope traces for aluminum targets. No energy-time focus was used.

Figures 5-1 and 5-2 (c) should be compared with Figure 3-7 (a) to see the great improvement obtained during the current contractual phase. Previously the Al^+ peak was smaller than either Na^+ or K^+, and could not be resolved from either. Even without energy-time focus, the present results clearly resolve all three peaks, and the plasma bubble temperature is much higher as evidenced by the ratios of the alkali metals to the aluminum peak.

The lower trace in these pictures provides a measure of the total number of single positive charges generated in the plasma bubble, that is, the number of ions if they are essentially all singly-charged. No multiply-charged ions were observed. The rise in the lower trace in the first microsecond determines the number of ions produced, being about 1×10^6 for Figure 5-1 and 2×10^6 for Figure 5-2 (c).

Although these present results show a resolution of masses 23, 27 and 39, the resolution is still not nearly adequate for a usable cometary particulate analyzer without energy-time focus.

5.2 DETERMINATION OF INITIAL CONDITIONS FOR COMPUTER SIMULATION

When the current results as shown in Figure 5-2 (c) without energy-time focus were compared with the results predicted by earlier computer simulations in Section 4.3, it was found that our earlier choices of initial conditions were incorrect. By picking new values for the three initial conditions of formation time distribution, initial velocity distribution, and initial position distribution, it was possible to match computer simulation results with experimental results. Such a match is demonstrated by comparing Figures 5-2 (a) and 5-2 (c) with respect to relative peak widths and positions (Aluminum target, 2500V at 46 cm).

58
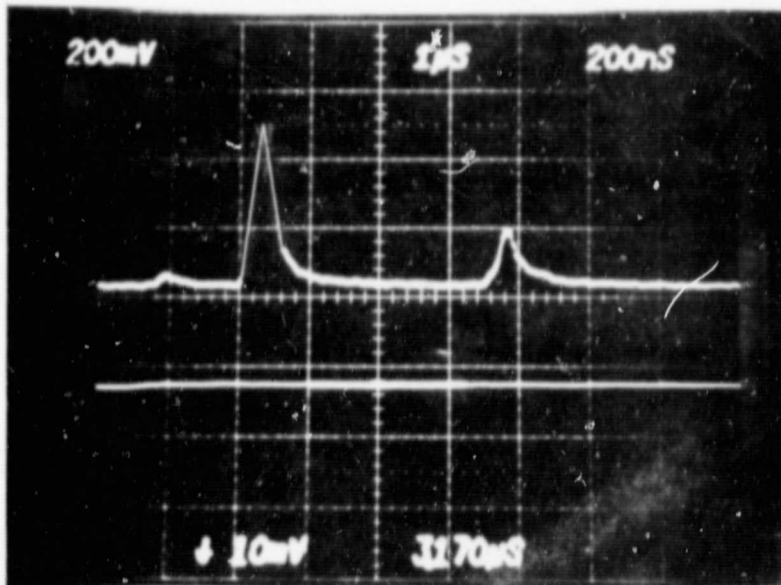
(a)
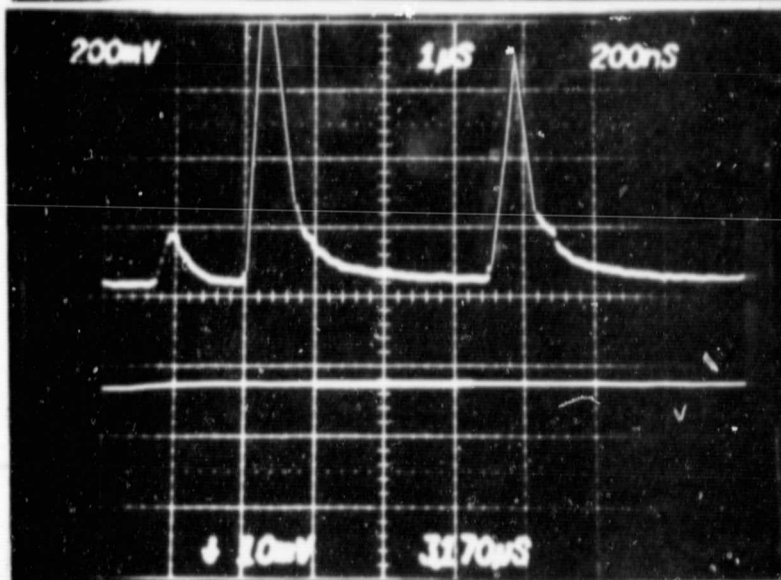
$Na^+(23)$, $Al^+(27)$, $K^+(39)$

Upper trace delay time: 3 μs
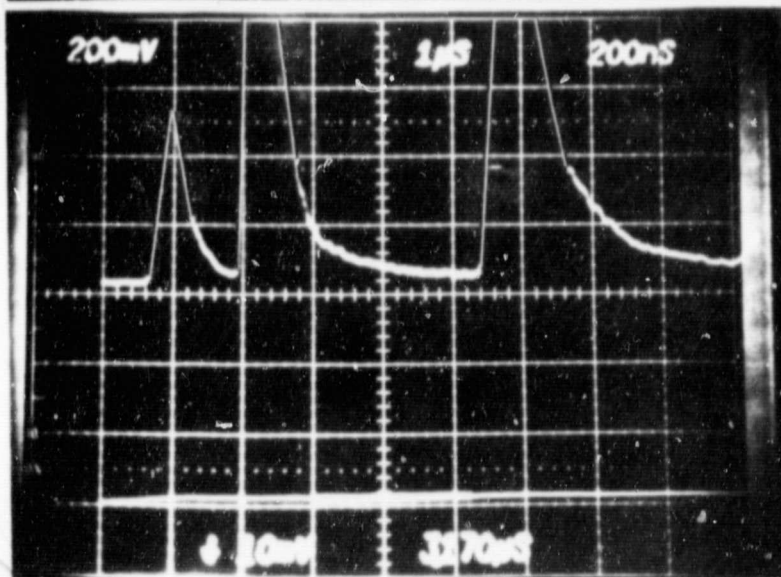Beam energy: 2500V
Flight path: 46 cm
Total number of ions: 1×10^6
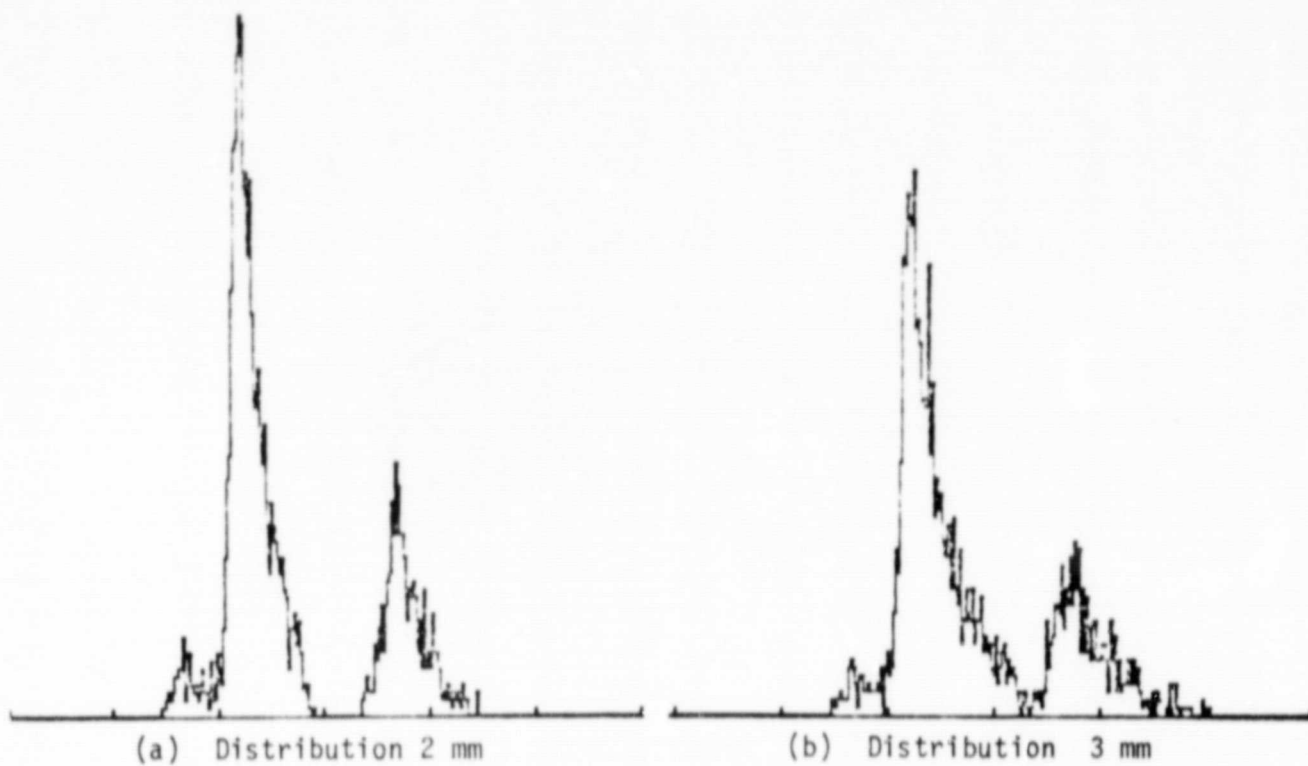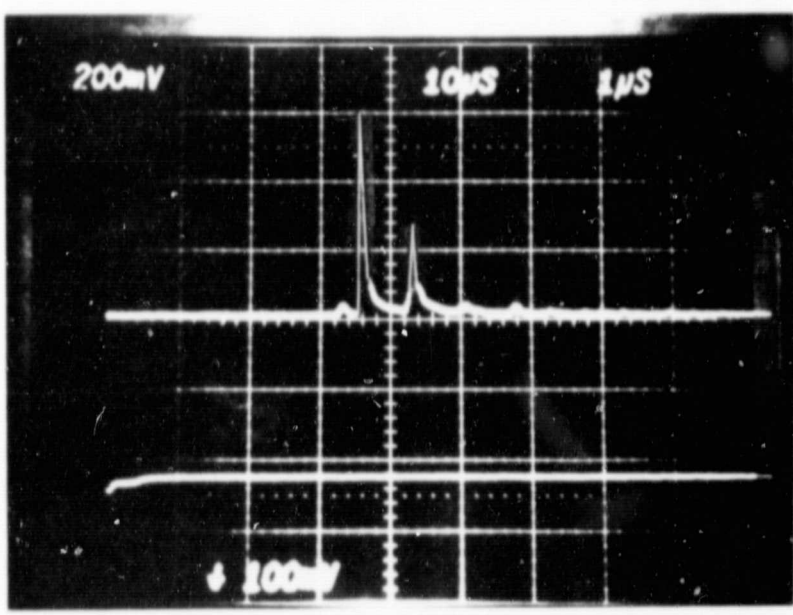Multiplier relative gain: 1

(b)

Multiplier relative gain: 2

(c)

Multiplier relative gain: 8

FIGURE 5-1. Mass Spectra from Aluminum Target: No Energy-Time Focus

(a) Distribution 2 mm

(b) Distribution 3 mm

(c) Experimental

FIGURE 5-2. Comparison of Computer Simulation and Experiment to Determine Initial Conditions

The current "best" choices consist of a uniform distribution of formation t_1 over 10 nanoseconds, an initial velocity distribution determined by a 20 eV temperature and "blow-off" parameter of 1.0 (see Section 4.3), and an initial position distribution given by an $x^{1/4}$ fall-off (i.e., $1-1.5 \, x^{1/4}$) from maximum to zero between the target and 2 mm away, with the acceleration plate 10 mm from the target. Figure 5-3 shows a Monte Carlo initial position distribution for 5000 particles, where the abscissa goes from zero to ten mm and the ordinate goes from 0 to 120 particles per 10 micrometer bin. Changing the zero point from 2 mm to 3 mm from the target makes the difference observed between Figures 5-2 (a) and 5-2 (b). In most results experimentally observed, the 2 mm case (Figure 5-2 (a)) was a good match. Occasionally, a value somewhat less would have matched better, but all the simulations to be compared with experiment here used the $x^{1/4}$ fall-off to zero at 2 mm. This is a significant change from the earlier simulations which required all ions to start within 0.5 mm of the target ($1-400 \, x^2$).

The change from a 30 nanosecond uniform formation time distribution to the current 10 ns is not significant, and the results for each are not significantly different. The value 10 ns was chosen since it corresponds to the laser pulse length. Some results with energy-time focus may indicate that 20 ns would be a better match. The greatest change from the earlier initial conditions is in initial ion kinetic energy, which has been changed from a temperature of 200 eV to 20 eV in order to match current experimental results. The simulation results at 20 eV are not very sensitive to a change in blow-off parameter from zero to one, but a value of one has been chosen as most realistic. The simulation results are quite insensitive to chosen temperature, with only minor change even with a 0.0 eV choice.
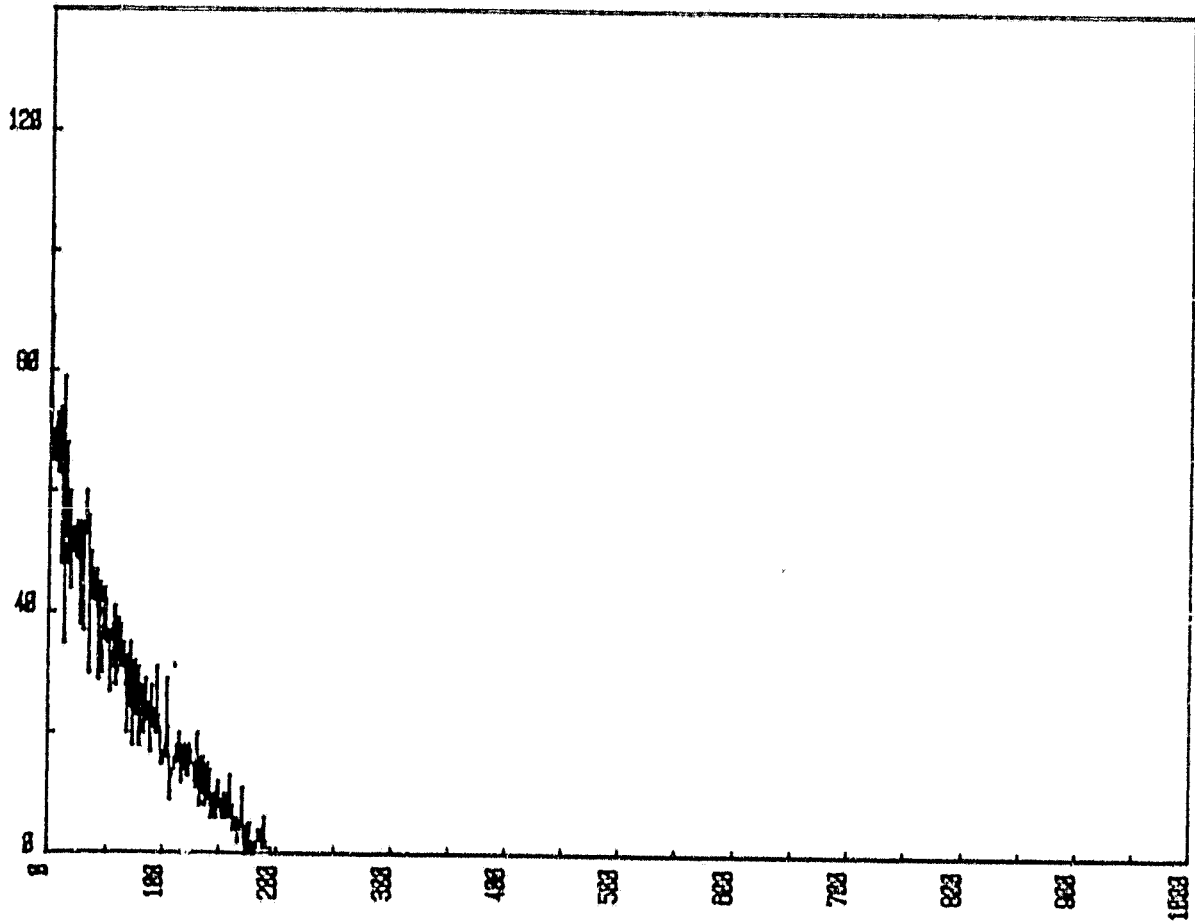
FIGURE 5-3. Monte Carlo Distribution of Initial Position of 5000 Ions.
Abscissa goes from 0 to 1.0 cm (target to acceleration
plate). Ordinate goes from 0 to 120 ions per 10 micrometer
bin.

Thus the initial conditions are dominated almost entirely by the initial position in the acceleration region. This is not too surprising in view of the resulting 400 eV spread compared to 2200 eV beam energy. This implies that even around 1×10^6 ions, the plasma bubble must reach the order of 1 mm size before it "goes free" in the acceleration field.

The great reduction in expected plasma bubble temperature from 200 to 20 eV apparently represents a real difference caused by the size of the bubble and number of particles present. Our earlier work on bigger bubbles definitely showed temperatures of hundreds of eV, and the current results with much smaller plasma bubbles show very much lower temperatures.

5.3   RESULTS WITH ENERGY-TIME FOCUS

Figure 5-4 (b) shows a computer simulation with energy-time focus "turned-on", using the initial conditions determined in Section 5.2. Table 5-1 lists the parameters used. Figure 5-4 (a) shows the experimental results obtained under corresponding experimental conditions. (All traces on polaroids in Section 5 have been enhanced where dim for reproduction). The full width at half maximum is 40 nanoseconds experimentally, while the computer simulation predicts about 20 ns. The overall shape and time dependence are excellent. The slight broadening may indicate some additional formation time spread, but the results are quite acceptable at this point in the development.
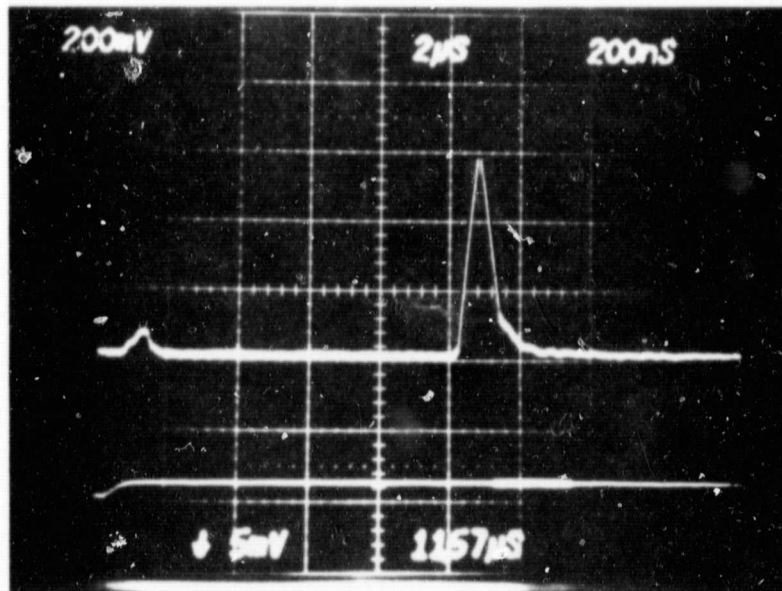
Figure 5-4 (c) shows the experimental effect of increasing the total number of ions per shot from 1×10^6 to 4×10^6 ions. This apparently results in "too big" a bubble.

(a)
1×10^6 Ions

(b)

Time Bins of Size 2 Nanosec

(c)
4×10^6 Ions
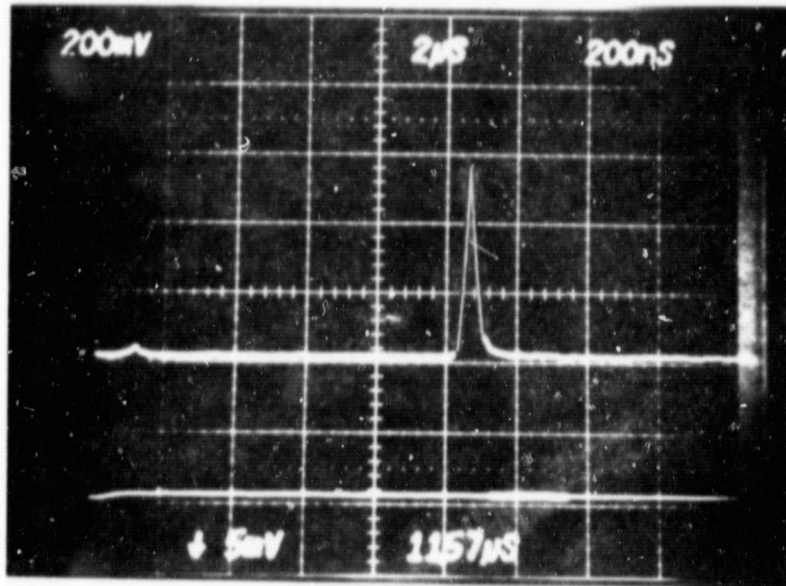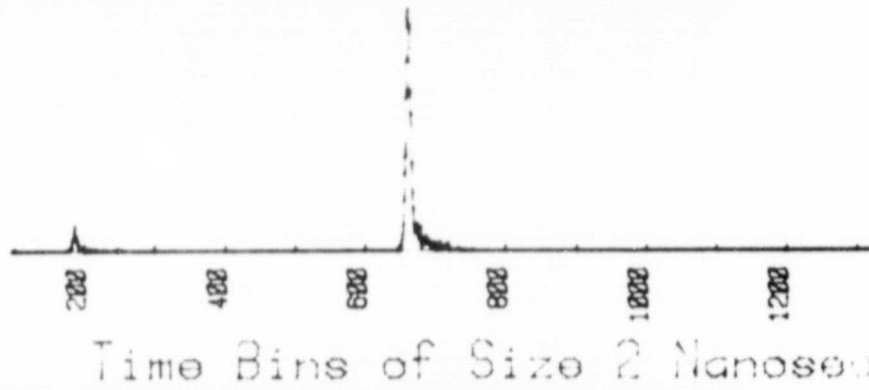
FIGURE 5-4. Comparison of Experimental Results with Computer
Simulation for Energy-Time Focus. Large peak is $Al^+(27)$
and the small peak is $Na^+(23)$. See Table 5-1 for
conditions.

64

TABLE 5-1

Ion masses and atom fractions:	7% mass 23^+, 93% mass 27^+
Total number of ions:	3000
Size of time bins:	2 nanoseconds
Region 1 potential difference:	3700 V
Energy after Region 2:	2200 eV
Region 1 length:	1.0 cm
Region 2 length:	1.4 cm
Region 3 length:	74 cm
Time pulse length:	10 nanoseconds
Initial position fall-off to zero	2 mm
Ion kinetic temperature	20 eV
Ion bubble cm lambda	1.0
Potential across reflection region	2820 V
Reflection parameter	3.8

Figure 5-5 shows a comparison of experimental results with a computer simulation, this time with a reflection parameter of 3.4 rather than the theoretically preferable 3.8. The experimental pulse shape changes less than the computer simulation predicts, but the overall agreement is excellent.

Figure 5-6 shows another comparison, this time over a greater part of the mass (time) spectrum. The three peaks are $Na^+(23)$, $Al^+(27)$ and $K^+(39)$. A hint of $K^+(41)$ may be seen. This Figure 5-6 should be compared to Figure 5-2 (c) to see the great gain in resolution due to the addition of energy-time focus described in Section 4.

Figure 5-7 shows results obtained under the same conditions as Figure 5-6, except that higher multiplier gains are used. Of particular interest are the peaks at 40 (Ca^+) and 41 (K^+), which should be 7% of the total K^+. Some of the smaller peaks are noise pulses because of the high multiplier gain.

Figure 5-8 shows the spectrum obtained for 304 stainless steel. The large peak to the left is impurity K^+ at mass 39 as usual, followed by 40 (Ca^+) and 41 (K^+). The large peak to the right is 52 (Cr^+), with nearby masses at 50 (Cr^+), 53 (Cr^+), 54 (Cr^+ and Fe^+), 55 (Mn^+), 56 (Fe^+, large peak), 57 (Fe^+ and something else), 58 (Ni^+) and 60 (Ni^+). The composition of 304 stainless steel should be around 20% chromium, 10% nickel, 2% manganese and 68% iron. The spectrum peak heights certainly don't show such a composition, and this is because of the difference in ionization potentials. Ionization potentials for Fe, Ni, Mn and Cr are 7.8, 7.6, 7.4 and 6.7 eV respectively. The relative peak heights for Fe and Ni are in about the right proportion, but Mn and particularly Cr are accentuated due to their lower ionization potentials. Chromium is enhanced by a factor of about 7 due to 1.1 eV lower ionization potential. Clearly the temperature of the plasma bubble is too low for satisfactory quantitative analyses.
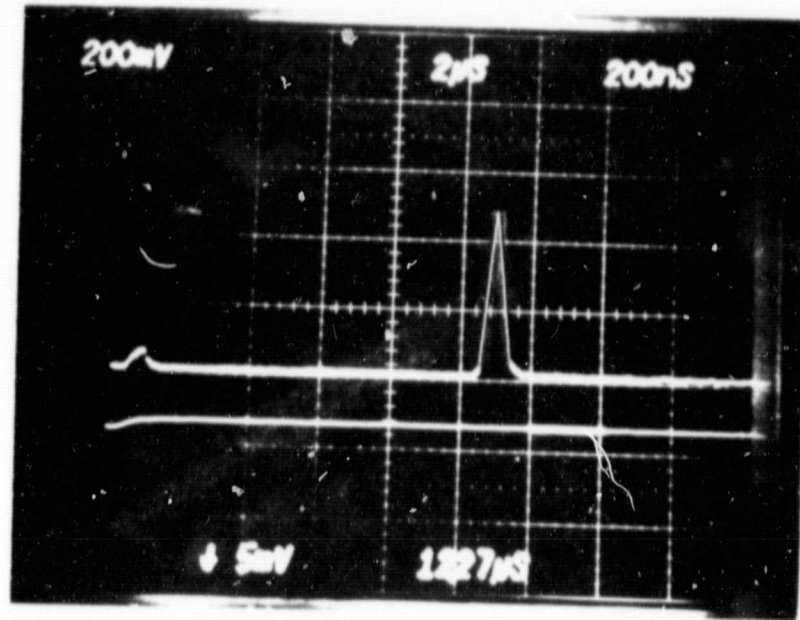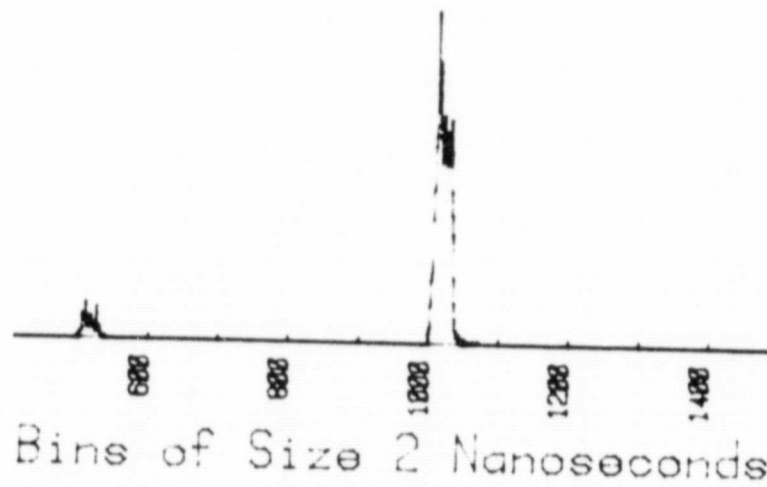
FIGURE 5-5. Comparison of Experimental Results with Computer Simulation.
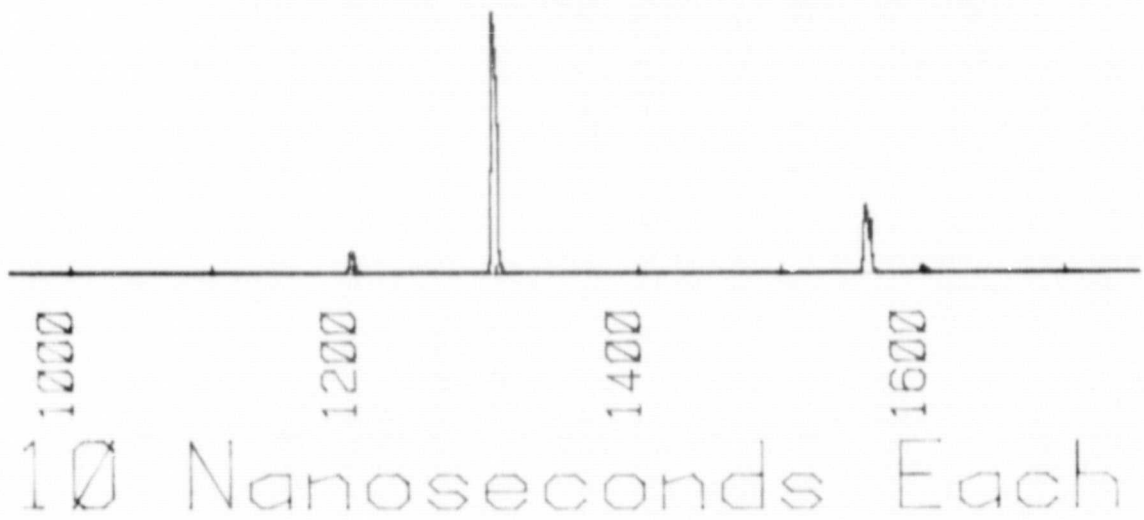The reflection parameter is 3.4 rather than the usual 3.8.

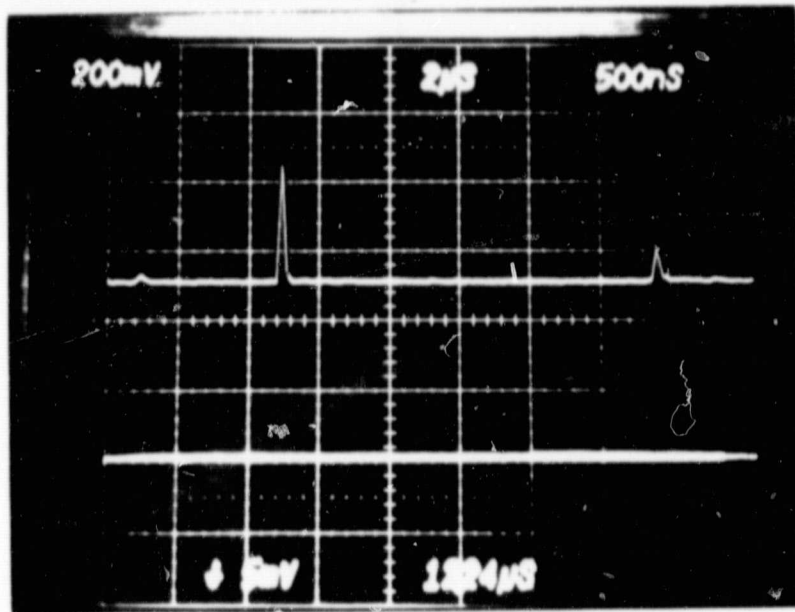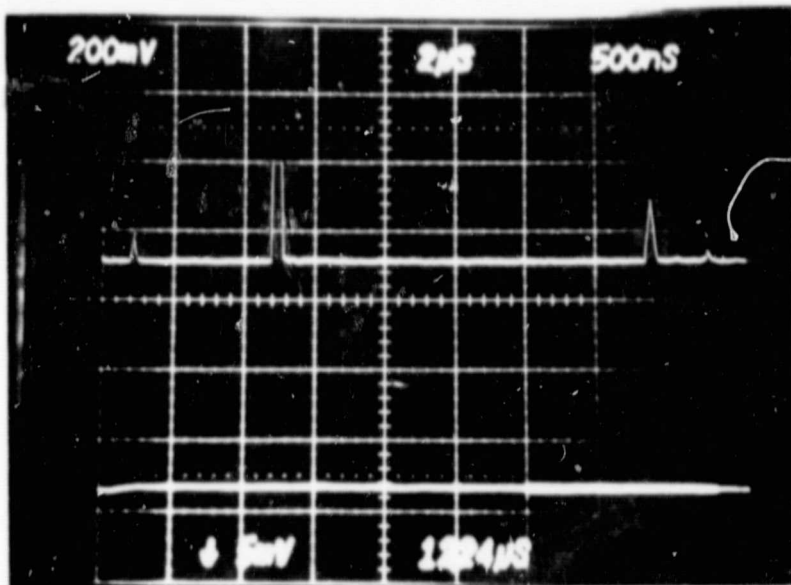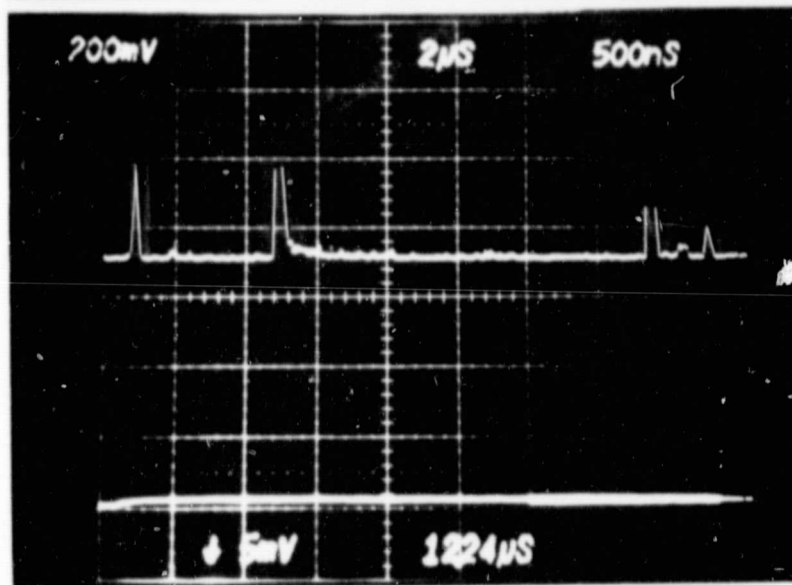FIGURE 5-6. Comparison of Experimental Results with Computer Simulation showing $Na^+(23)$, $Al^+(27)$ and $K^+(39)$.

(a)
Relative gain: 2
(to Figure 5-6)

(b)
Relative gain: 6

(c)
Relative gain: 20

FIGURE 5-7.   Spectra from Aluminum Target.   Photo (c) shows peaks at
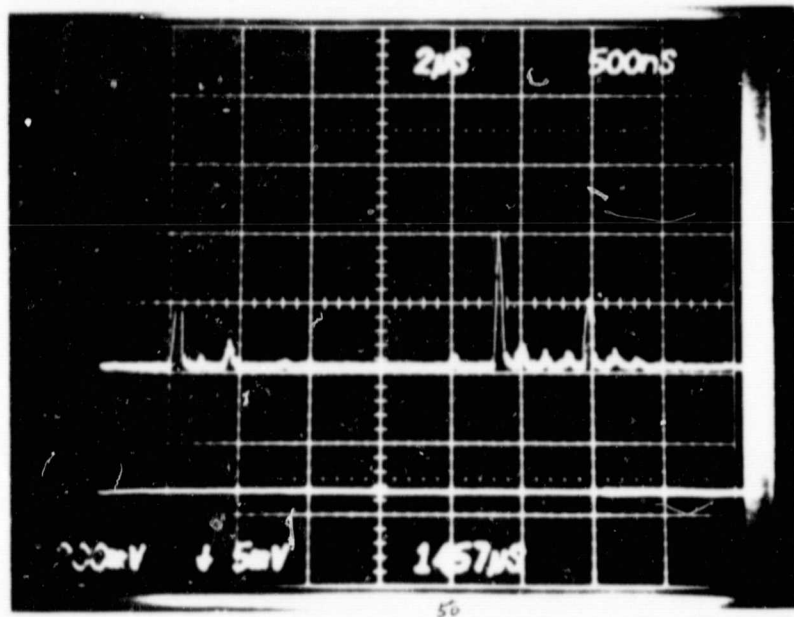23 (Na$^+$), 27 (Al$^+$), 39 (K$^+$), 40 (Ca$^+$), 41 (K$^+$).

FIGURE 5-8. Spectrum of 304 Stainless Steel. Largest peak to the right is mass 52 (Cr^+), with 50 (Cr^+), 53 (Cr^+), 54 ($Cr^+ + Fe^+$), 55 (Mn^+), 56 (Fe^+), 57 ($Fe^+ + ?$), 58 (Ni^+), 60 (Ni^+)

Figure 5-9 shows the spectrum of silver compared to a computer simulation based on the usual initial conditions. Silver has two isotopes, 51% at mass 107 and 49% at mass 109. The instrument sensitivity is poor, and the statistical noise due to individual ions is evident. The computer simulation used 200 ions total, which seems to match reasonably, implying only a few hundred of the initial 10^6 ions are reaching the detector. Resolution is quite satisfactory.
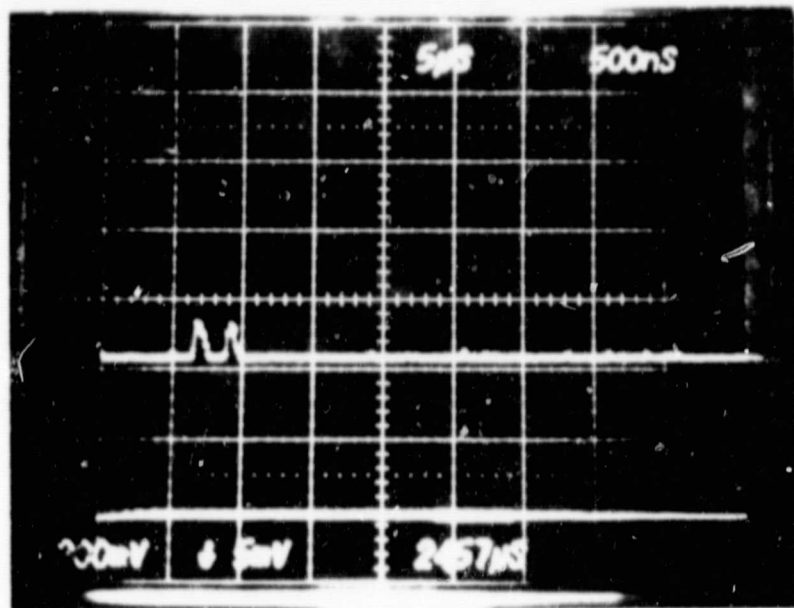
Figure 5-10 shows a computer simulation for a spectrum of 50% mass 250 and 50% mass 251, as expected using the usual initial and experimental conditions. It is seen that 250 and 251 would be resolved.

5.4   DISCUSSION OF CURRENT RESULTS

The current results show a great improvement in mass resolution through the use of energy-time focus. With the present experimental parameters, and keeping the total number of ions no larger than 1×10^6 per shot, it may be concluded that adequate mass resolution has been achieved.

Two serious problems remain: poor ion transmission and inadequate plasma bubble temperature. It appears e.g., that only 10^{-4} of the silver ions reach the detector. The present apparatus includes clearly insufficient ion beam focus. Unless some subtle ion loss is present, it will not be difficult to design and construct adequate ion beam focus and steering electrodes for the system. This is a first necessity in the next phase of the instrument development.

The second problem, low plasma bubble temperature, will be attacked by changing the laser beam focusing lens from 100 mm focal length to 50 mm focal length to decrease the spot size. This will increase the power density by 4 times thereby reaching 10^{10} watts/cm^2, while maintaining ion numbers at 10^6. Whether this will be sufficient to reduce the sensitivity to ionization potential cannot be predicted, and only experiment can say how much sensitivity to ionization potential will remain. Calibration with samples similar to cometary particulates is expected to allow adequate quantitative analysis for many purposes.
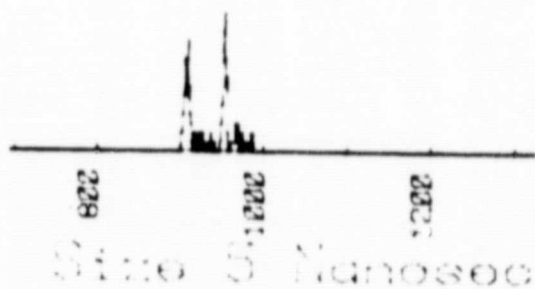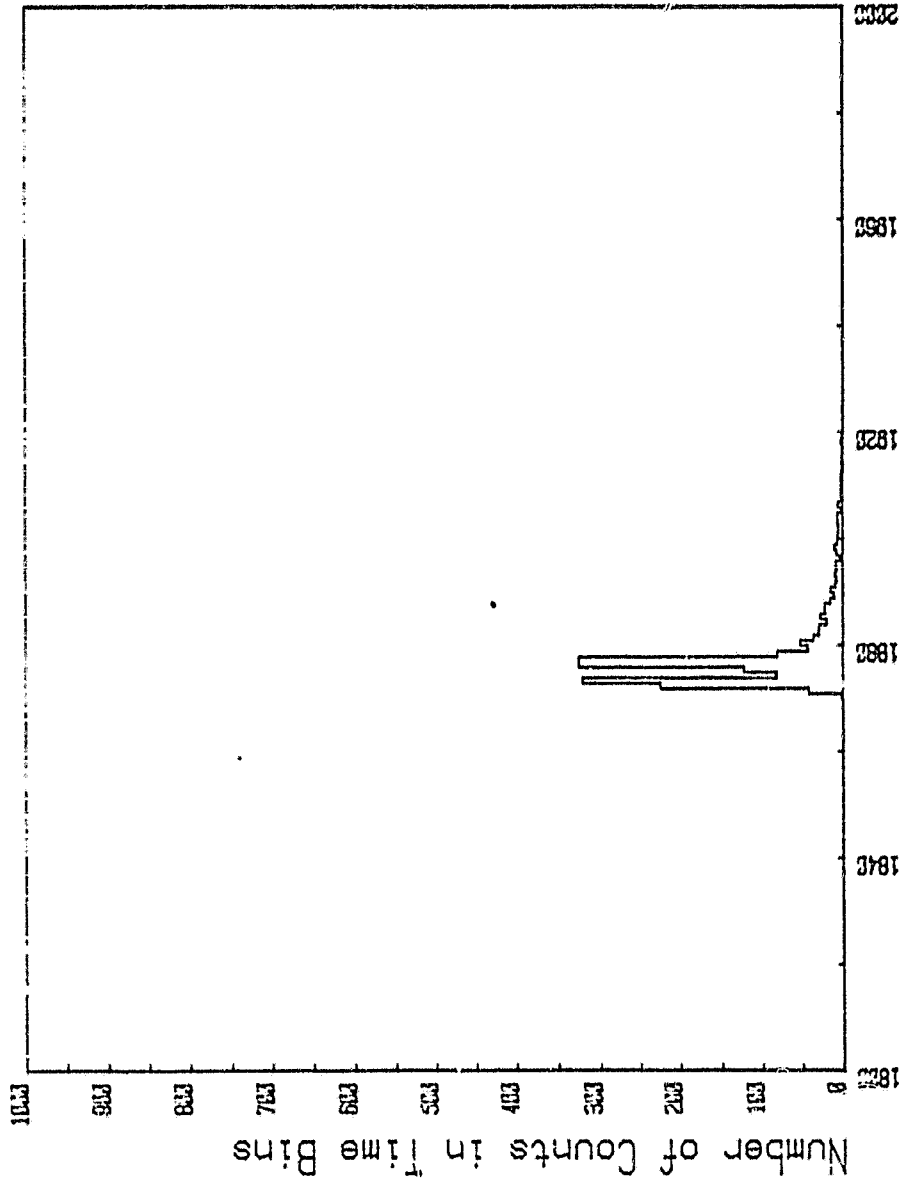
FIGURE 5-9. Spectrum of Silver, 51% at Mass 107 and 49% at Mass 109, and Comparison with Computer Simulation

FIGURE 5-10.   Computer Simulation for Spectrum of 50% Mass 250 and 50% Mass 251

Of utmost importance in the next phase after sensitivity and plasma bubble temperature have been increased, is the analysis of geochemical samples to see how much quantitative data can be obtained from such complex targets. It is expected that geochemists will be utilized heavily during such experiments.

Nothing has been said or done so far here about using negative ions. Negative ions have been used in analyses by the German LAMMA group with considerable success. In this case high bubble temperature is not as essential, and with minor modifications, our instrument should be convertible to positive or negative ions. Negative ions are potentially of particular importance in analyzing such species as oxygen which have high ionization potentials compared to metals, and which form negative ions. Molecular species may also be amenable to negative ion analysis.

These current findings, combined with the results of other workers in the field as described in recent publications, provide strong evidence as to the feasibility of the CPA concept. There are, of course, a number of engineering design problems to be solved and there must be an extension of the present work to more adequately demonstrate the definitive nature of the results that could be expected from a flight experiment.

6.0 BASELINE INSTRUMENT SPECIFICATIONS

6.1 SUMMARY OF LASER BLOW-OFF COMETARY PARTICULATE ANALYZER

Instrument Type:	Time-of-flight ion mass spectrometer
Ion Source Type:	Pulsed laser surface vaporization and ionization
Sampled Area:	5 μm diameter spot
Sampled Depth:	1 μm depth
Mass Range:	1 to 250 AMU
Mass Resolution:	1 at 250 AMU
Flight Path:	1 meter total, folded in instrument
Laser Type:	Nd-YAG, Q-switched, 10 ns pulse
Laser Energy:	1 mJ per pulse
Data Rate:	20 ns time bins (50 megahertz sample digitizing)
Data Buffer:	2048 x 8 bit bins, dumped after each laser pulse
Laser Pulse Rate:	0.1 per second
Instrument Power:	10W average; 25W peak
Instrument Mass:	12 kg
Sample Collection:	Surfaces with collected samples, and standards transported to instrument from view port and storage.
RF Fields:	Negligible
Magnetic Fields:	Static negligible; small pulsed field with pump lamp discharge

6.2 INSTRUMENT MECHANICAL SPECIFICATIONS

The major mechanical development involves sample and standards handling. It is planned to utilize a storage cassette in which standards carriers and exposed sampling surface carriers can be stored until they are individually transported to the laser-lens focal plane for analysis. Such a storage capability is highly advantageous in that samples and standards can be returned to for further comparison after real time earth-based consideration.

The major "new technology" development involves the laser. However, it appears that this is well in hand with the laser from International Laser Systems (Orlando, FL) (10 cm x 7 cm x 3 cm), light (0.3 kg), rugged, low power Q-switched Ng-YAG laser which appears to meet the necessary specifications. It will be possible to carry two individual lasers for redundancy with minor penalty.

The entire instrument package will have dimensions approximately 30 cm x 30 cm and a length between 50 and 100 cm, depending on the degree of flight path folding which can be accomplished.

6.3 INSTRUMENT ELECTRONICS AND DATA HANDLING (PROPOSED)

The electronic subsystem (ESS) provides the instrument regulated power, signal acquisition, conditioning and conversion, data processing, storage and formatting, and command and control functions.

A block diagram of the ESS is shown in Figure 6-1. The ESS is microprocessor (μP) based and all sequencing, control and data handling functions are under μP control.

The time-of-flight (TOF) data sensed by the EMT is amplified and then digitized by alternating 8-bit ADCs each operating at a 25 megasample/second conversion rate for an effective rate of 50 megasamples/second. The time between successive samples is about 20 nanoseconds. Samples are stored in two 1K x 8 RAMs with a 25 nanosecond access (write cycle) time. The ADC words are fully buffered so a new conversion takes place while the previous word is being transferred to memory. The ADC is thus allowed to operate at its maximum conversion rate.

At the end of each laser pulse the 2048 samples stored in fast RAM are transferred to low power system RAM and power is removed from the fast clock circuitry, the fast ADCs and fast RAMs. This fast circuitry consumes about 15 watts when on. Since it is only required for milliseconds at a time, power switching greatly reduces the average power. A separate 12-bit ADC is used to digitize various engineering/ housekeeping measurements which are also stored in system RAM. Upon command from the spacecraft the science and engineering data are transferred in bit-serial fashion to the spacecraft telemetry system.

Each science data collection cycle is initiated by firing one of the two redundant lasers. The laser control circuitry in turn initiates the fast ADC conversion cycles which continue until all 2048 samples have been stored.

The motor controllers control stepper motors which position and focus the sample holders. The controllers act in accordance with external commands via the microprocessor.

The high voltage supplies are programmable and are adjusted in accordance with external commands. The low voltage power supply generates all of the instrument circuit voltages.

This supply provides its outputs anytime the nominal 28 volt bus is present at its input terminals.
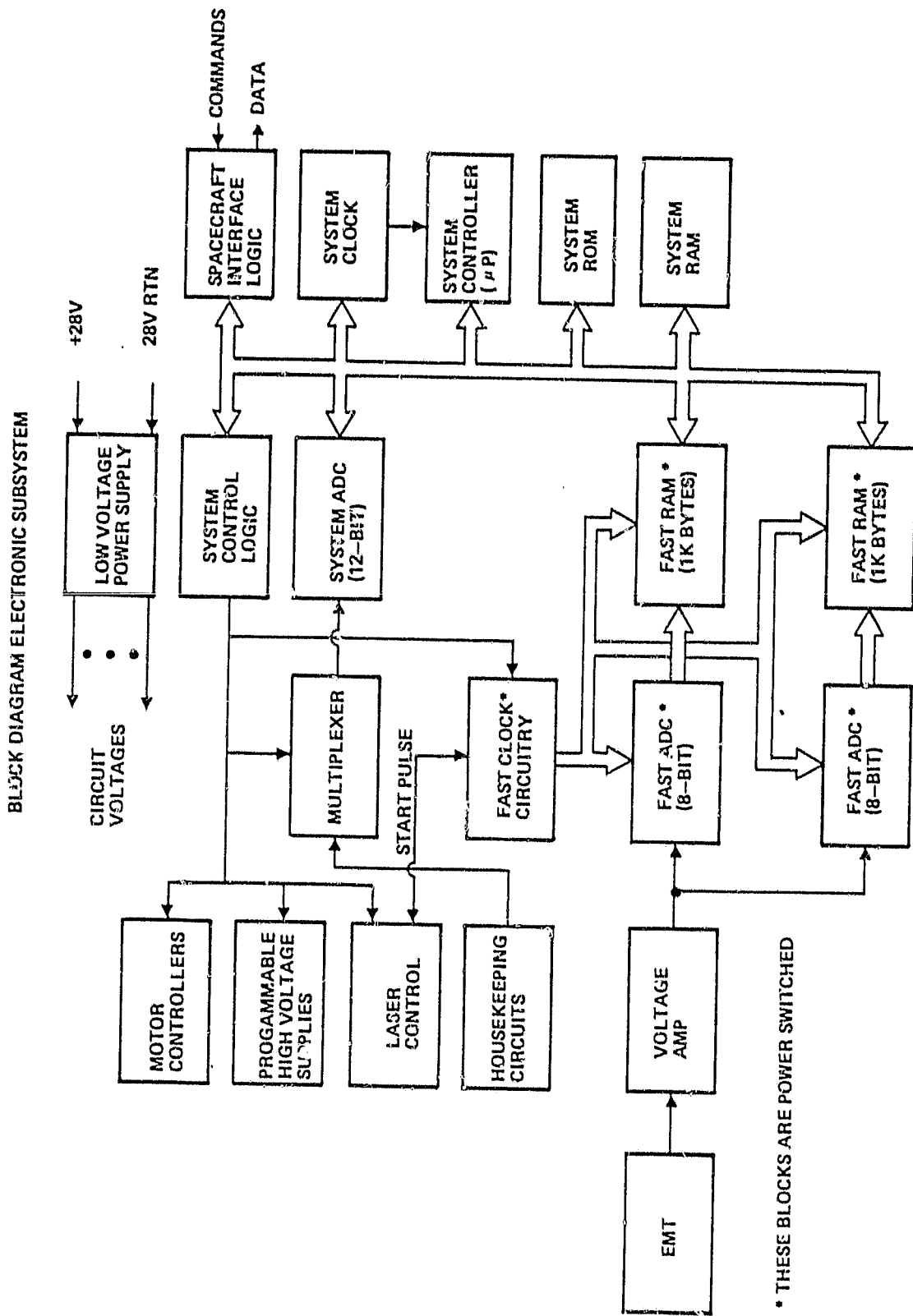
BLOCK DIAGRAM ELECTRONIC SUBSYSTEM

FIGURE 6-1. Block Diagram Electronic Subsystem

* THESE BLOCKS ARE POWER SWITCHED

78